# EVALUACIÓN DE LA TECNOLOGÍA “FAST VALVING” APLICADA A UNA PLANTA DE VAPOR DE 900MW PARA MANTENER LA ESTABILIDAD TRANSITORIA DEL SISTEMA ELÉCTRICO.

**RICARDO ANTONIO DOMÍNGUEZ GÓMEZ**

**UNIVERSIDAD INDUSTRIAL DE SANTANDER**
**FACULTAD DE INGENIERIAS FISICO-MECÁNICAS**
**ESCUELA DE INGENIERIA ELÉCTRICA, ELECTRÓNICA Y TELECOMUNICACIONES E3T**
**BUCARAMANGA, COLOMBIA**
**2013**

# EVALUACIÓN DE LA TECNOLOGÍA "FAST VALVING" APLICADA A UNA PLANTA DE VAPOR DE 900MW PARA MANTENER LA ESTABILIDAD TRANSITORIA DEL SISTEMA ELÉCTRICO.

**RICARDO ANTONIO DOMÍNGUEZ GÓMEZ**

**Trabajo de Grado para optar al título de Ingeniero Electrónico**

**Director**
**HERMANN VARGAS TORRES**
**PhD. Ingeniería Eléctrica**

**Co-Director**
**RUDY CEPEDA GÓMEZ**
**PhD. Ingeniería Mecánica**

**UNIVERSIDAD INDUSTRIAL DE SANTANDER**
**FACULTAD DE INGENIERIAS FISICO-MECÁNICAS**
**ESCUELA DE INGENIERIA ELÉCTRICA, ELECTRÓNICA Y TELECOMUNICACIONES E3T**
**BUCARAMANGA, COLOMBIA**
**2013**

## TABLE OF CONTENTS


Paper: *ASSESSMENT OF FAST VALVING TECHNOLOGY FOR A STEAM POWER PLANT AS SUPPORT TO THE POWER SYSTEM STABILITY* ..... 12

I. INTRODUCTION ..... 12

II. FAST VALVING ..... 12

*a) Actuation* ..... 13

*b) Modeling* ..... 14

III. DESCRIPTION OF STUDY SYSTEM ..... 14

IV. RESULTS OF THE STUDY ..... 14

V. CONCLUSIONS ..... 18

REFERENCES ..... 18

ANNEX I: MODEL OF THE STEAM TURBINE ..... 19

*I.I Physical description* ..... 19

*I.II Mathematical model of ST* ..... 20

*I.III Implementation of ST in MatLab/Simulink and SimPowerSystems toolbox* 23

ANNEX II: THEORY OF SYNCHRONOUS MACHINES ..... 27

*II.I Physical description* ..... 27

*II.II Mathematical model of Synchronous Machine* ..... 29

*II.III Steady-state analysis* ..... 37

*II.IV Implementation of Synchronous Machines in MatLab/Simulink and SimPowerSystems toolbox* ..... 40

ANNEX III: THEORY OF EXCITATION SYSTEMS AND *PSS* ..... 51

*III.I Excitation Systems* ..... 51

*III.II Power System Stabilizers* ..... 54

*III.III Tuning of Excitation System and PSS* ..... 57

ANNEX IV: TUNING OF THE *ST* SPEED GOVERNOR ..... 64

ANNEX V: *FAST VALVING* CONTROL ..... 75

ANNEX VI: EFFECTS OF *FV* ON THE *ST* AND ITS CONTROL SYSTEM ..... 79

*VI.I Mechanical integrity of the valves* ..... 80

*VI.II Mechanical integrity of the turbine* ..... 81

REFERENCES ..... 83

## LIST OF FIGURES


Fig. 1 Valve stroke characteristic. ..... 13
Fig. 2 Typical variation of *RACKE* and $\omega$. ..... 13
Fig. 3 Power load unbalance ..... 14
Fig. 4 Mathematical model of *FV* control. ..... 14
Fig. 5. Diagram of the study system. ..... 14
Fig. 6 Angular rotor angle variations for *FCT* at *t* = 82,0926 *ms* ..... 15
Fig. 7 Angular rotor angle variations for *FCT* at *t* = 90,3614 *ms* ..... 15
Fig. 8 Angular rotor angle variations for *FCT* at *t* = 93,2947 *ms* ..... 15
Fig. 9 Angular rotor angle variations for *FCT* at *t* = 101,7191 *ms* ..... 15
Fig. 10 Acceleration power for *FCT* at *t* = 82,0926 *ms* ..... 15
Fig. 11. Acceleration power for *FCT* at *t* = 90,3614 *ms* ..... 16
Fig. 12. Acceleration power for *FCT* at *t* = 93,2946 *ms* ..... 16
Fig. 13. Accelerating power for *FCT* at *t* = 101,7191 *ms* ..... 16
Fig. 14. Mechanical power and the valve strokes for *FCT* at *t* = 82,0926 *ms* with *Efd* constant ..... 16
Fig. 15. Mechanical power and the valve strokes for *FCT* at *t* = 90,3614 *ms* with *AVR* ..... 16
Fig. 16. Mechanical power and the valve strokes for *FCT* at *t* = 93,2946 *ms* with *AVR* and PSS ..... 17
Fig. 17. Mechanical power and valve stroke for *FCT* at *t* = 101,7191 *ms* with *AVR, PSS* and *FV* ..... 17
Fig. 18. Speed deviation for *FCT* at *t* = 82,0926 *ms* with *Efd* constant ..... 17
Fig. 19. Speed deviation for *FCT* at *t* = 90,3614 *ms* with *AVR* ..... 17
Fig. 20. Speed deviation for *FCT* at *t* = 93,2946 *ms* with *AVR* and *PSS* ..... 17
Fig. 21. Speed deviation for *FCT* at *t* = 101,7191 *ms* with *AVR*, *PSS* and *FV* ..... 17
Fig.AI. 1. Scheme of tandem-compound *ST* with single *RH* configuration ..... 20
Fig.AI. 2. Steam Vessel Model ..... 21
Fig.AI. 3. Steam Turbine model ..... 23
Fig.AI. 4. Default model of *ST* implemented by *SimPowerSystems* toolbox ..... 24
Fig.AI. 5. Customized model of tandem-compound *ST* with single *RH* implemented in *SimPowerSystems* ..... 25
Fig.AI. 6. Default model of speed governor implemented in *SimPowerSystems* ..... 25
Fig.AI. 7. *CV* stroke vs. Flow characteristic curve
Fig.AI. 8. *IV* stroke vs. Flow characteristic curve ..... 26
Fig.AI. 9. Model of servomotors customized for *CV* and *IV* ..... 26
Fig.AII. 1. Schematic diagram of a three-phase synchronous machine ..... 28
Fig.AII. 2. Ideal machine representation ..... 30
Fig.AII. 3. Electrical model of the synchronous machine ..... 33
Fig.AII. 4. Representation of dq components of armature voltage and currents as phasors ..... 37
Fig.AII. 5. Steady state phasor diagram ..... 39
Fig.AII. 6. Transformation from *abc* frame to *qd rotating* frame applying Eq.AII.4b. ..... 40
Fig.AII. 7. Transformation from *qd rotating* frame to *abc* frame applying Eq.AII.4a. ..... 41

Fig.AII. 8. Block to create the current faults. ..... 41
Fig.AII. 9. D-axis equations diagram blocks ..... 42
Fig.AII. 10. Q-axis equations diagram blocks ..... 43
Fig.AII. 11. Electrical equations diagram blocks ..... 44
Fig.AII. 12. Mechanical equations diagram blocks ..... 45
Fig.AII. 13. Complete system block diagram of the synchronous machine ..... 46
Fig.AII. 14. Block diagram of infinite bus ..... 47
Fig.AII. 15. Block diagram of electrical model of synchronous machine in SimPowerSystems toolbox ..... 49
Fig.AII. 16. Internal block diagram of Synchronous Machine Continues Model in SimPowerSystems toolbox ..... 50
Fig.AII. 17. Block diagram of mechanical model of synchronous machine in SimPowerSystems toolbox ..... 50
Fig.AIII. 1. General functional block diagram for synchronous machine excitation control system ..... 51
Fig.AIII. 2. Terminal voltage transducer and optional load compensation elements 52
Fig.AIII. 3 Excitation System Type DC1A – DC Commuter exciter ..... 53
Fig.AIII. 4 PSS Type PSS1A – Single input ..... 54
Fig.AIII. 5. The excitation model implemented by *SimPowerSystems* ..... 56
Fig.AIII. 6. The *PSS* model implemented by *SimPowerSystems* ..... 57
Fig.AIII. 7. Bode diagram of a well-tuned *DC1A* excitation system model. ..... 58
Fig.AIII. 8. Terminal Voltage open-circuit step response of *DC1A* model. ..... 61
Fig.AIII. 9. Field Voltage open-circuit step response of *DC1A* model ..... 62
Fig.AIII. 10. Responses of *PSS* with tuned and default values without disturbance applied. ..... 63
Fig.AIII. 11. Responses of *PSS* with tuned and default values with disturbance applied at *t*=80ms. ..... 63
Fig.AIV. 1. Scheme for tune a controller of one plant ..... 64
Fig.AIV. 2. Response curve in S-shape for tune a controller ..... 65
Fig.AIV. 3. Diagram block to tune the controller for a plant ..... 66
Fig.AIV. 4. Diagram for tune the controller with Ziegler-Nichols method ..... 67
Fig.AIV. 5. Output of step input with open loop ..... 67
Fig.AIV. 6. Analysis of curve fitted described by Eq. AIV.5 ..... 69
Fig.AIV. 7. Response curve of the speed governor, tangent line at infection point and steady value to find L and T values ..... 71
Fig.AIV. 8. Responses of the types of controllers proposed by Ziegler and Nichols and the SimPowerSystems by default ..... 72
Fig.AIV. 9. Responses of PID proposed by Ziegler and Nichols and the PID tuned by *PID tuner* toolbox ..... 73
Fig.AV. 1. *(a)* Responses of *delay block (b)* Responses of *integrator block* ..... 76
Fig.AV. 2. Responses of the first blocks and operator in the upper part of the *FV* mathematical model ..... 77
Fig.AV. 3. Responses of the blocks and operators in the lower part of the *FV* mathematical model ..... 78

## LIST OF TABLES

TABLE I Valves stroke characteristic times ..... 14
TABLE II Differents *CCT* for each condition. ..... 15
TABLE AII I Subscripts of variables to describe the synchronous machine model .. 33
TABLE AII II Usual short circuit currents and powers for different line voltage values ..... 49
TABLE AIV. I Ziegler-Nichols tuning rules based on slope input to a plant ..... 65
TABLE AIV. II Values of parameters for the differents types os controllers proposed by Ziegler and Nichols ..... 71
TABLE AIV. III Performance and robustness of every type of controller studied .... 73
TABLE AIV. IV Porcentage of improvement on the performance of the *PID* controllers ..... 74

## RESUMEN ESPAÑOL

**TITULO:** EVALUACIÓN DE LA TECNOLOGÍA “FAST VALVING” APLICADA A UNA PLANTA DE VAPOR DE 900MW PARA MANTENER LA ESTABILIDAD TRANSITORIA DEL SISTEMA ELÉCTRICO. *

**AUTOR:** RICARDO ANTONIO DOMÍNGUEZ GÓMEZ. **

**PALABRAS CLAVES:** *Fast Valving, Estabilidad Transitoria de Sistemas de Potencias, Planta de Energía a Vapor, MatLab/Simulink/SimPowerSystems, Turbina a Vapor, Generador*.

Esta investigación consta de un artículo científico, donde sugiere la técnica de control Fast Valving (FV) como un efectivo, económico y adaptable medio para mejorar y apoyar los márgenes de estabilidad transitoria del sistema, cuando una planta de energía a vapor es usada.

Su desempeño es comparado contra controles primarios del sistema, como lo son el Regulador Automático de Voltaje (AVR, por sus siglas en inglés) y el Estabilizador de Sistemas de Potencia (PSS, por sus siglas en inglés), además del controlador primario de velocidad de la turbina. Esta comparación es llevada a cabo a través de la herramienta computacional MatLab/Simulink/SimPowerSystems.

El sistema a considerar es una planta de energía a vapor conformada por una turbina a vapor y un generador de 900MW conectados a un sistema de maquina sencilla y bus infinito (SMIB, por sus siglas en inglés). A través de la plataforma de simulaciones, se aplicarán diferentes fallas y así se mostrará como FV mejora dichos márgenes de estabilidad transitoria, basándose en el comportamiento de sus señales tales como la desviación del ángulo del rotor, la potencia mecánica aplicada a la turbina, la potencia eléctrica del generador, la potencia de aceleración así como también la desviación de velocidad sufrida por el rotor.

---

***** Trabajo de Investigación

** Facultad Fisicomecanicas. Escuela: Eléctrica, Electrónica y Telecomunicaciones.
Director: Hermann Vargas Torres. Codirector: Rudy Cepeda Gómez.

## ABSTRACT IN ENGLISH

**TITLE:** ASSESSMENT OF FAST VALVING TECHNOLOGY FOR A STEAM POWER PLANT OF 900MW AS SUPPORT TO THE POWER SYSTEM STABILITY. *

**AUTHOR:** RICARDO ANTONIO DOMÍNGUEZ GÓMEZ. **

**KEY WORDS:** *Fast Valving, Power System Stability, Steam Power Plant, MatLab/Simulink/SimPowerSystems, Steam Turbine, Generator.*

This research developed a paper where is suggest the Fast Valving (FV) control technique as an effective, inexpensive, and adaptable mean to improve and support the power system stability margins when a steam Power Plant (PP) is used.

Its performance is compared versus primary controls of the system like Automatic Voltage Regulator (AVR) and Power Systems Stabilizer (PSS). The comparison is carried out with MatLab/Simulink.

The model considers a Steam Power Plant consisting of a 900MW Steam Turbine (ST) and a Generator (Gen) connected to a Single Machine–Infinite Bus system (SMIB). The simulation platform applies several faults and then shows how FV improves the transient stability margins, based on the behavior of the Gen as the rotor angle deviation, the mechanical power supplied to the ST, the electrical power of the Gen, the acceleration power and also the speed deviation experienced by the rotor.

---

* Research Thesis

** Faculty Physicomechanical. School: Electrical, Electronic and Telecommunications Engineering.

Tutor: Hermann Vargas Torres. Tutor: Rudy Cepeda Gómez.

# Assessment of Fast Valving Technology for a Steam Power Plant as Support to the Power System Stability

Domínguez, Ricardo., Cepeda, Rudy., Vargas, Hermann.
*Escuela de Ingeniería Eléctrica, Electrónica y Telecomunicaciones, Universidad Industrial de Santander.*
*Bucaramanga, Colombia*
ricardominguez@ingenieros.com, rudycepeda@gmail.com, hrvargas@uis.edu.co

***abstract — this paper suggests the Fast Valving (FV) control technique as an effective, inexpensive, and adaptable mean to improve and support the power system stability margins when a steam Power Plant (PP) is used. Its performance is compared versus primary controls like Automatic Voltage Regulator (AVR) and Power Systems Stabilizer (PSS). The comparison is carried out with MatLab/Simulink. The model considers a Steam Power Plant consisting of a 900MW Steam Turbine (ST) connected to a Single Machine–Infinite Bus system (SMIB). The simulation platform applies several faults and then shows how FV improves the transient stability margins.***

***Keywords —Fast Valving, Power System Stability, Steam Power Plant, Matlab/Simulink/SimPowerSystems***

## I. INTRODUCTION

The concentration of synchronous machines may lead to stability problems in post-fault conditions in case of a failure near to them. A loss of synchronism can be caused by high active power infeed of the mechanical energy stored during the voltage drop until the clearing of the short circuit [1]. The longest fault duration time not resulting in instability, is referred as the critical clear time (*CCT*). When the fault clear time (*FCT*) is longer than *CCT* the generator (*Gen*) loses synchronism with the rest of the system and starts an asynchronous (out-of-step) operation. The asynchronous operation is not permissible due to the thermal effect of large currents, large power and voltage swings in the network and the adverse effect on stability of other *Gen* [2].

For these reasons, new requirements and additional strict rules have been developed to support the system stability. New and old *PP* must implement new control systems to fulfill these new and stricter grid codes.

There are several different ways to study the stability of power systems. This work focuses on the electromechanical part to analyze the effects of *FV*.

During the steady state operation of a power system, the mechanical power ($P_m$) and the electrical power ($P_e$) are in equilibrium. This means that the *Gen* performs synchronously as shown by the backswing equation. The simplest form of this equation is:

$$\frac{2H}{\omega_0}\frac{d^2\delta}{dt^2} = P_a = P_m - P_e \qquad (1)$$

Where $H$ is the *Gen* inertia constant, $\omega_0$ is the nominal speed and $\delta$ is the rotor angle and $P_a$ the acceleration power.

When a severe and sudden failure occurs, $P_e$ drops and swings, while at the same time $P_m$ is reduced slowly and slightly by the governor and primary control action of the *ST*. When this occurs the $P_a$ value rises, putting the synchronous performance at risk. This effect can be explained under the *equal area criterion* [2,3,4]

One method to avoid the speeding up of the machine is to reduce $P_m$ as soon as possible, trying to keep it in a range of values similar to the $P_e$ drop. In this way, $P_a$ remains within admissible values. This can be achieved reducing the steam supply by a fast closing and reopening of the *ST* valves. This control technique is known as *Fast Valving*. *FV* is one of the most effective, adaptable, inexpensive and proven methodologies to maintain synchronism without *Gen* tripping, reducing $P_m$ for a defined time to keep the *Gen* acceleration in an acceptable range [1].

## II. FAST VALVING

*FV* is one of the discrete supplementary control (*DISCOS*) techniques used to improve the power systems stability. *DISCOS* are designed for non-continuous use and are only complementary rather than primary controllers [5].

*FV* acts directly on the control valves (*CV*) and/or intercept valves (*IV*) omitting the *ST* control. It enables a rapid control of the $P_m$ produced by the *ST*, which is delivered to the *Gen*. Thus, *FV* leads to a reduction of $P_a$ in case of a failure [1]. The fast closure must be initiated in the shortest possible time after the detection of a meaningful disturbance, and must be followed by the reopening of the valves.

Since reheaters (*RH*) have large physical dimensions, a large amount of steam is stored in their interiors. Then, even with a fast closure of the *CV*, the *ST* still supplies about 0,7 p.u. of power through the intermedium pressure (*IP*) and low

pressure (*LP*) stages. This is caused by the expansion of steam stored in the *RH* to the inferior pressure stages. That means, the *IV* controls nearly 70% of the total unit power, whereas *CV* controls the remaining 30% from the high pressure (*HP*) stage. When only the *IV* is actuated, *FV* is known also as Early Valve Actuation (*EVA*) [3]. Larger power reduction can be obtained by integrating both, *CV* and *IV* together.

*FV* can be classified into two categories: Momentary Fast Valving (*MFV*) and Sustained Fast Valving (*SFV*), which can be differentiated through the valve position as shown in Fig.1. In *MFV*, the valves are fully reopened after a total or partial closure initiated by the fault detection. If the valves only reopen partially after the total or partial closure, the actuation is known as *SFV* [3].

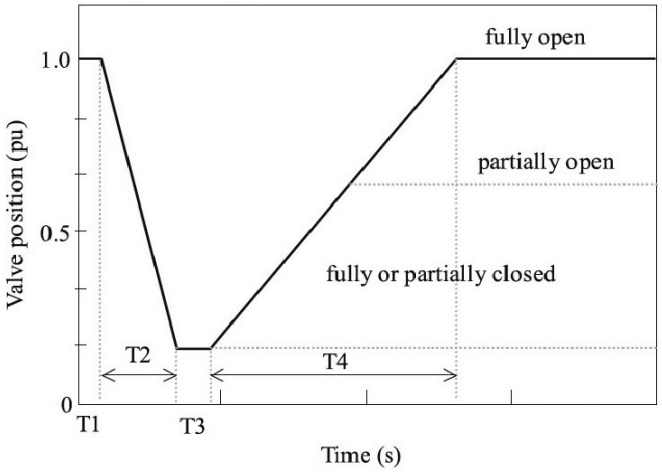


Fig. 1 Valve stroke characteristic [6].

In Fig.1, $T_1$ is the delay between the starting time and the time when the valve begins to close, $T_2$ is the valve closing time, $T_3$ is the time during which the valve remains closed, also known as dead time and $T_4$ is the valve reopening time.

The impact of *FV* on system stability strongly depends on the speed of closing and reopening, which is determined by the governor system used. A common practice is the utilization of fast-acting hydraulic valves arranged to dump oil from the spring-loaded actuating cylinders of the valves. If applications require faster reopening, special technology with hydraulic accumulators can be used [1].

Some of the primary limitations of the conventional *FV* schemes include valve opening and closing rate constraints and valve dead time, which is not adjustable to very low values [7]. Too long reopening times may also create difficulties. They may lead to an enhancement of the backswing of the *Gen*, causing synchronism losses [1].

*a) Actuation*

The activation of *FV* can be triggered by different signals, the relationship between $P_m$ and $P_e$, the speed deviation ($\Delta\omega$), and the conjunction of the angular speed ($\omega$) with $P_a$ being the most important.

In previous works [8,9], the rate of change of kinetic energy (*RACKE*) of the rotor mass and the $\Delta\omega$ signals were effectively used to decide the best sets of valve closing / opening criteria. From (1), the *RACKE* equation is:

$$RACKE = \omega P_a \tag{2}$$

Fig. 2 shows the normal trend for *Gen* in any power system. A close look to Fig. 2 reveals that the frequency of variation of *RACKE* is twice that of $\omega$. Therefore, the valve closing can be initiated when $\Delta\omega$ has a positive value. Similarly, the valve opening can be initiated when $\Delta\omega$ changes from positive to negative. Thus, for all practical purposes, the $\Delta\omega$ can be used to guide the opening and closing of the turbine valves. This further simplifies the control strategy and minimizes the measuring and computational requirements. A deeper explanation can be found in [6,8,9].

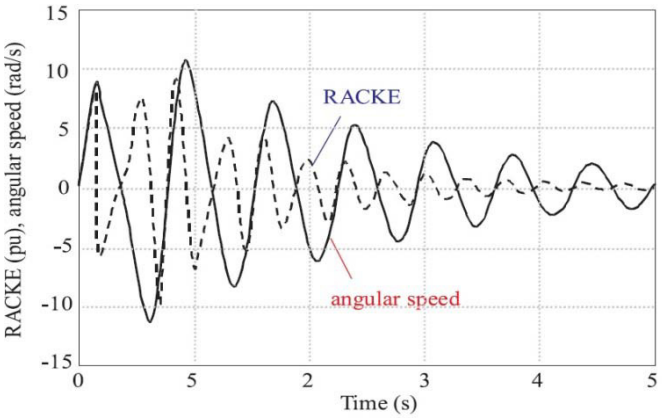


Fig. 2 Typical variation of *RACKE* and $\omega$ [8].

The criteria can be summarized as below:

*Valve Closing Criterion:*

$$RACKE = 0 \quad and \quad \Delta\omega = 0\pm\uparrow \tag{3}$$

Where, $0\pm\uparrow$ means that the variable is zero while changing sign from negative to positive.

*Valve Opening Criterion:*

$$RACKE = 0 \quad and \quad \Delta\omega = 0\pm\downarrow \tag{4}$$

Where, $0\pm\downarrow$ means that the variable is zero while changing sign from positive to negative [6].

When the acceleration is within certain lower limits, the operation of the *FV* may not be necessary. To avoid this, another device, such as Power Load Unbalance (*PLU*), described in Fig. 3, can be used to discriminate between severe and not severe faults. The circuit turns on whenever the *Gen* output power decreases faster than a preset rate and $P_m$ exceeds $P_e$ by an amount $K$ that could be set by the turbine user [3].

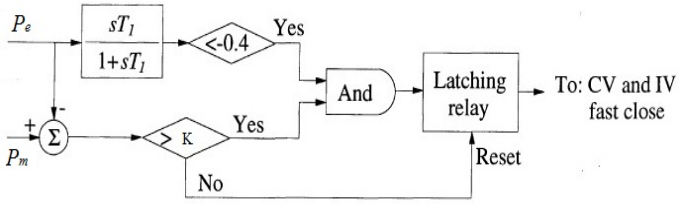


Fig. 3 Power load unbalance [4].

*b) Modeling*

We implemented a mathematical model that describes the valve stroke characteristic curve when *FV* is actuating as shown in Fig 1.

The block diagram represents the *SFV* model. To obtain the *MFV* mathematical model it is necessary to change some parameters [3].

The input is the *FV* trigger signal. It comes from the S-R flip-flop, which guarantees that *FV* actuates only once after the signal have been launched.

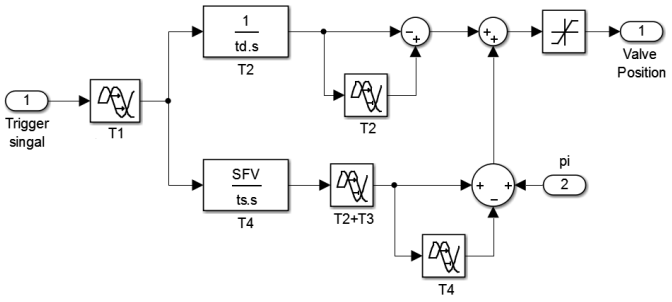


Fig. 4 Mathematical model of *FV* control.

The block diagram described in Fig. 4 contains the different times delays from Fig. 1 summarized in table I.

TABLE I.
VALVES STROKE CHARACTERISTIC TIMES

| *Times* | *Values (s)* |
|---|---|
| T1 | 0,1 |
| T2 | 0,1 |
| T3 | 0,2 |
| T4 | 8 |

*SFV* indicates the final position of the valve, varying from 0 to 1. If it is 1, *SFV* becomes immediately to *MFV*. The limits of the saturation limiter are also between 0 to 1.

## III. DESCRIPTION OF STUDY SYSTEM

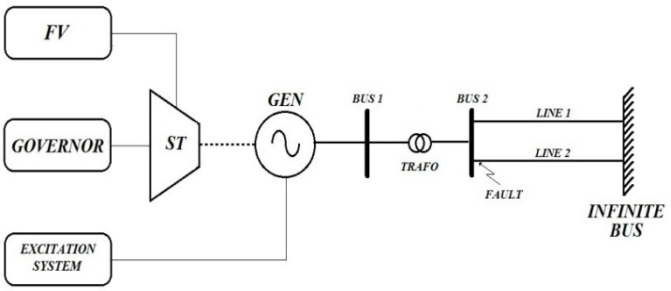


Fig. 5. Diagram of the study system.

Fig. 5 shows the scheme used to simulate the system employing the toolbox in MatLab/Simulink called *SimPowerSystems*. It consists of a *SMIB* system of a steam *PP* with a *ST*, its speed governor/primary control, *Gen* with its excitation system, including an *AVR* plus a *PSS* and a *FV* control system added to the *ST*. The *PP* generates 900MW and all its parameters correspond to those of an actual industrial model described in Fig 5.

The system to study is an adaptation of a German grid, with 50Hz. The *Gen* is a 3-phase, round-rotor, synchronous machine, represented by a sixth-order state-space model with 1175 MVA, 27kV, 900MW and 0,80p.f, as main features. The *ST* is single *RH* tandem-compound type, with its main stages: *HP, IP* and *LP.* The Governor is an electro-hydraulic control, with the basic elements as speed governor, speed relays, and hydraulic servomotors [4].

The excitation system consists of *AVR* and *PSS*. The *AVR* is a DC1A type and the *PSS* is a PSS1A type, both models recommended for stability studies by [10].

These models are models implemented in the *SimPowerSystems* toolbox of MATLAB/Simulink, but were modified in order to adapt and implement the *FV* control scheme.

The system undergoes a three-phase fault at the line 2 at $t = 0{,}5\ s$ and we study the behavior of the synchronous machine under the following conditions:

- With $E_{fd}$ constant
- With *AVR*
- With *AVR* and *PSS*
- With *AVR, PSS* and *FV* actuation

## IV. RESULTS OF THE STUDY

The simulation results were made and applied to one system *SMIB* and under the conditions described above.

By means of simulations for each condition, the following *CCT* in table II were obtained.

TABLE II.
DIFFERENTS *CCT* FOR EACH CONDITION

| *Conditions* | *CCT (ms)* | *% Increase* |
|---|---|---|
| $E_{fd}$ cte | 82,0925 | - |
| *AVR* | 90,3613 | 9,03\| |
| *AVR + PSS* | 93,2946 | 12,5693 |
| *AVR + PSS +FV* | 101,7190 | 23,9079 |

The angular variations for different *FCT* and for each condition are shown in Fig. 6 to Fig. 9.

For each case, when the *FCT* exceeds the *CCT* of the system, the value of the rotor angle increases fast getting out quickly of the range of accepted values. The machine gains speed and may lose synchronism, putting at risk the whole system operation.

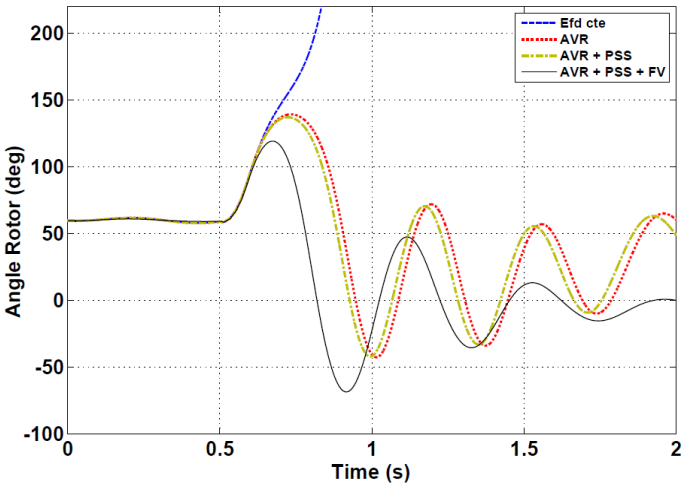


Fig. 6 Angular rotor angle variations for *FCT* at $t$ = 82,0926 *ms*

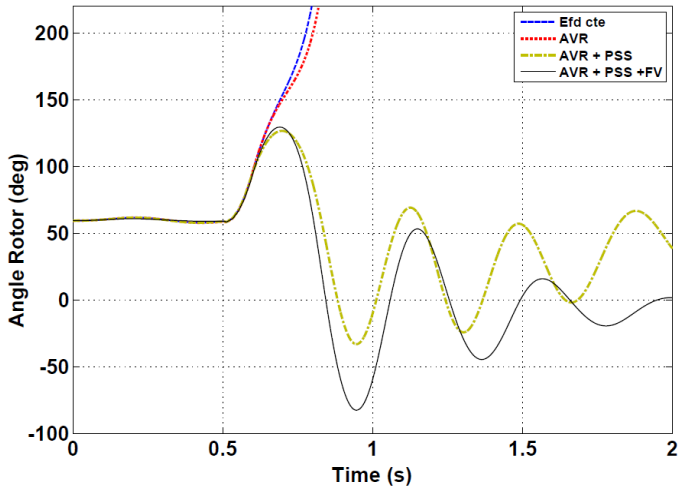


Fig. 7 Angular rotor angle variations for *FCT* at $t$ = 90,3614 *ms*

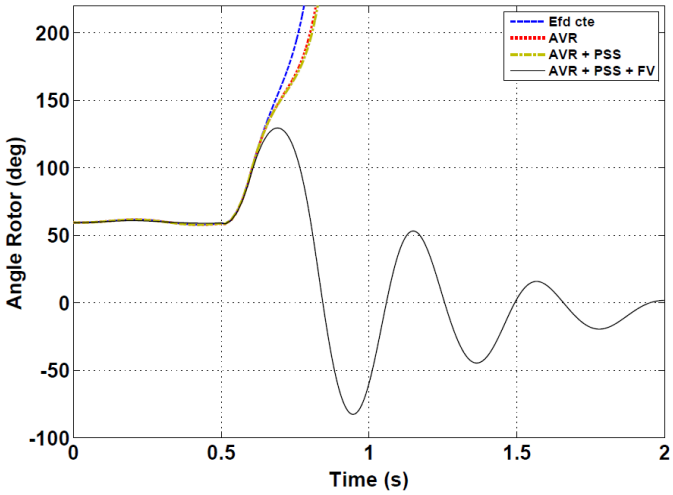


Fig. 8 Angular rotor angle variations for *FCT* at $t$ = 93,2947 *ms*

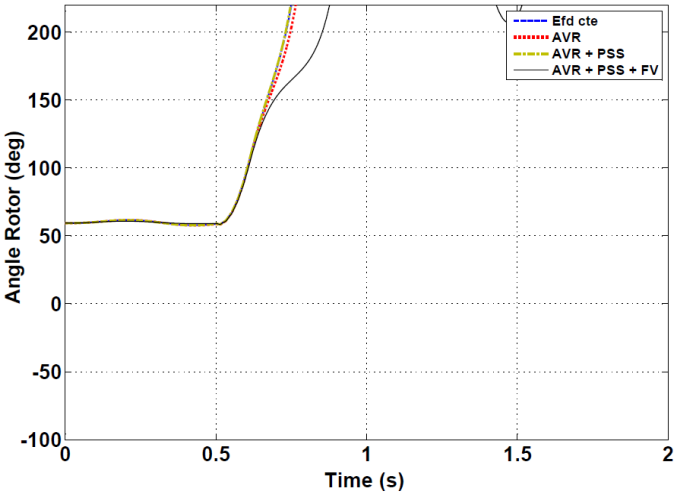


Fig. 9 Angular rotor angle variations for *FCT* at $t$ = 101,7191 *ms*

This is also reflected in the $P_{a,}$ which comes from the difference between the $P_e$ generated by the *Gen* and the $P_m$ supplied by the *ST* as shown in (1). The $P_a$ for the same *FCT* and under same conditions are shown in Fig. 10 to Fig. 13.

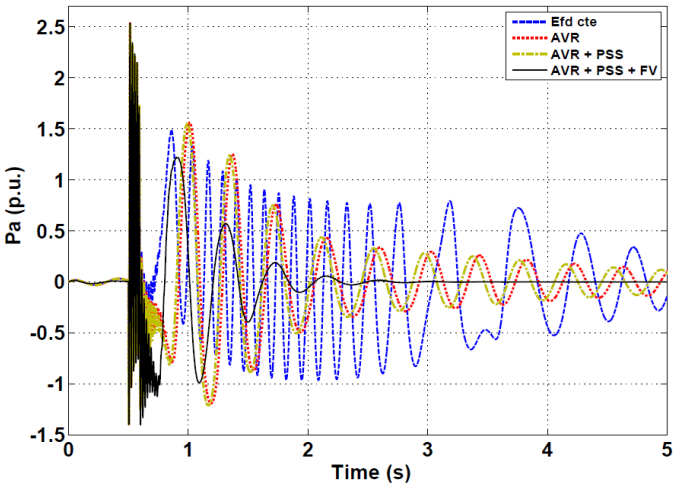


Fig. 10 Acceleration power for *FCT* at $t$ = 82,0926 *ms*

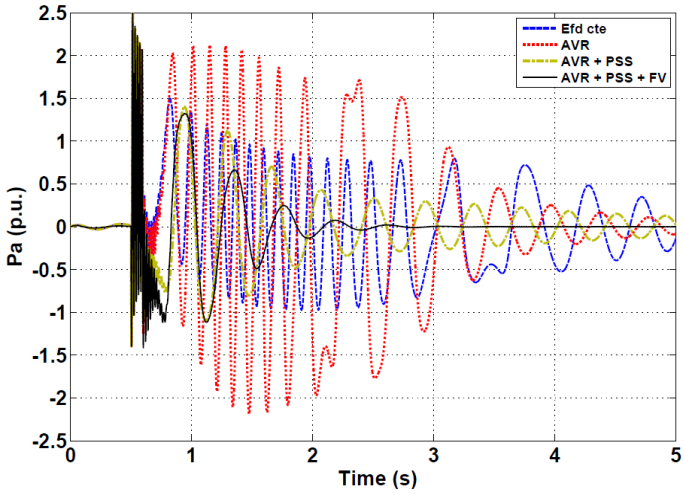


Fig. 11. Acceleration power for *FCT* at $t$ = 90,3614 *ms*

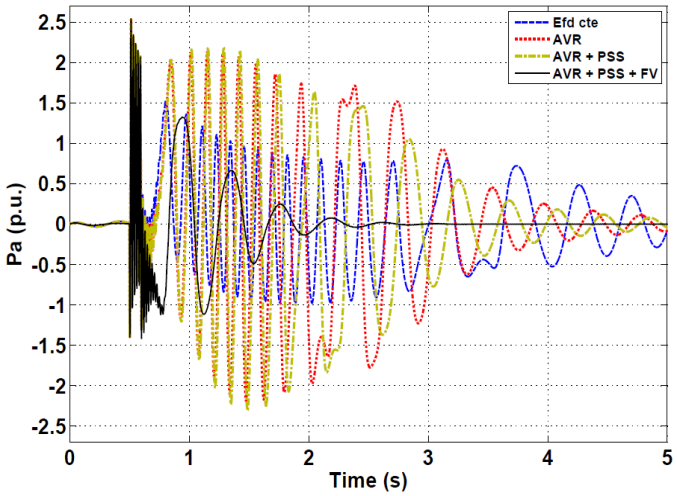


Fig. 12. Acceleration power for *FCT* at $t$ = 93,2946 *ms*

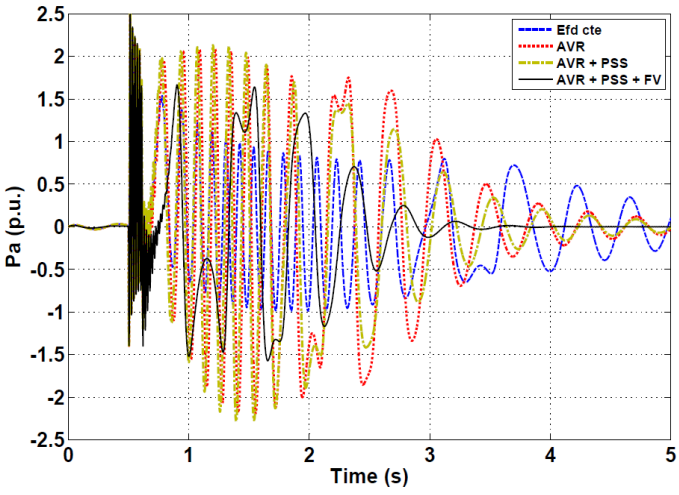


Fig. 13. Accelerating power for *FCT* at $t$ = 101,7191 *ms*

When the fault occurs and while it is cleaned, the *FV* actuation causes larger variations in $P_a$ causing vibration on the shaft, which is not recommended. After that period, *FV* damped these values due to the reduction of mechanical torque input to the generator. The reduction of the mismatch between $P_a$ and $P_e$ and is greater compared with the other conditions.

Fig. 14 to Fig. 17 show how is the behavior of the $P_m$ versus the valves stroke. In cases when the *FV* control system is not being applied, the responsible of the reduction of speed is the governor. It is not able to close the valves as soon as *FV* can do it. Figures 14 to 17 describe this behavior.

Another way to demonstrate how *FV* improves and enhances the stability margins and supports the net is with the signal of damping of the deviation speed. This relationship is presented in Fig. 18 to Fig. 21.

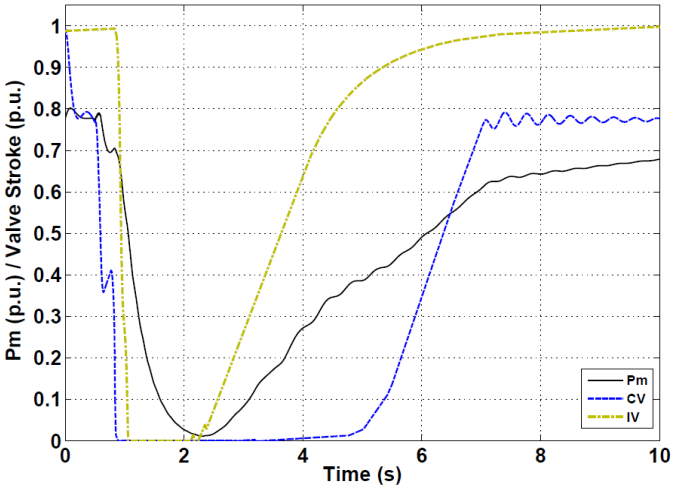


Fig. 14. Mechanical power and the valve strokes for *FCT* at $t$ = 82,0926 *ms* with *Efd* constant

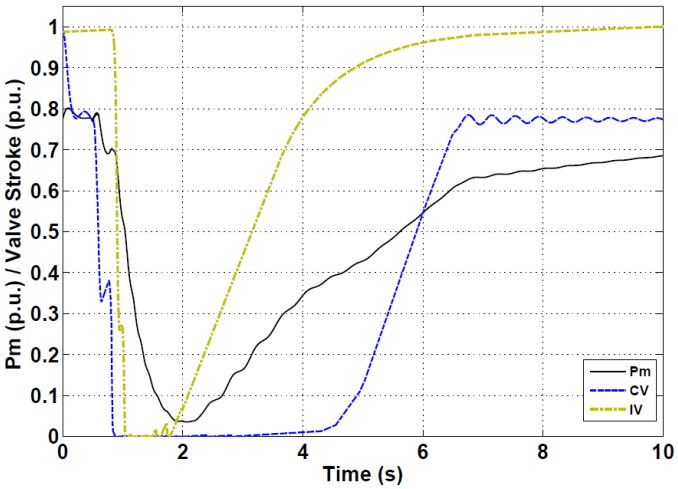


Fig. 15. Mechanical power and the valve strokes for *FCT* at $t$ = 90,3614 *ms* with *AVR*

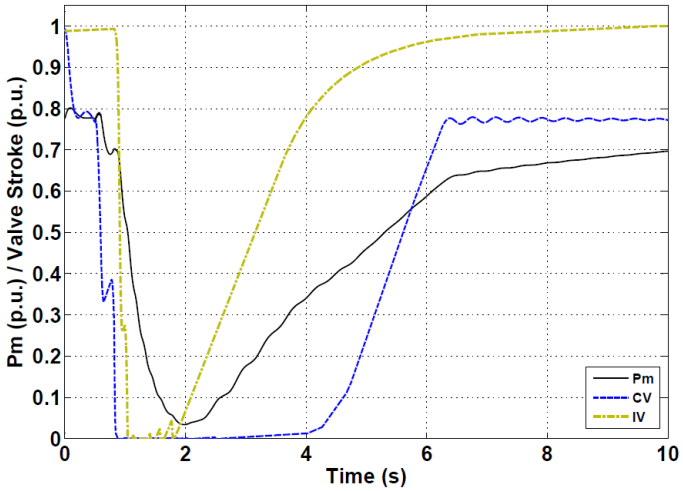


Fig. 16. Mechanical power and the valve strokes for *FCT* at $t$ = 93,2946 *ms* with *AVR* and PSS

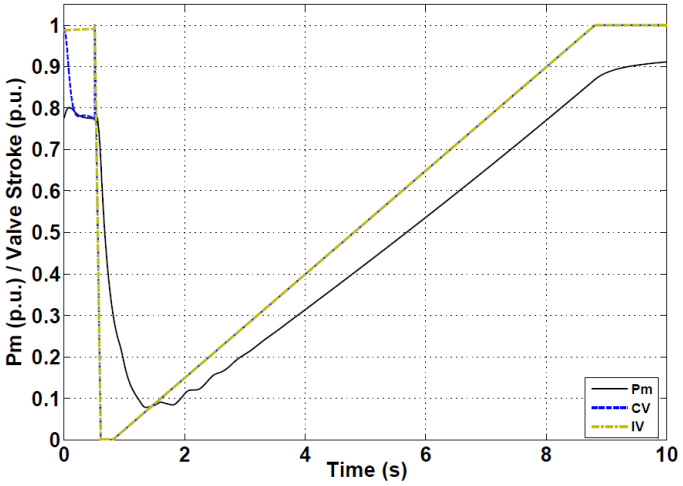


Fig. 17. Mechanical power and valve stroke for *FCT* at $t$ = 101,7191 *ms* with *AVR, PSS* and *FV*

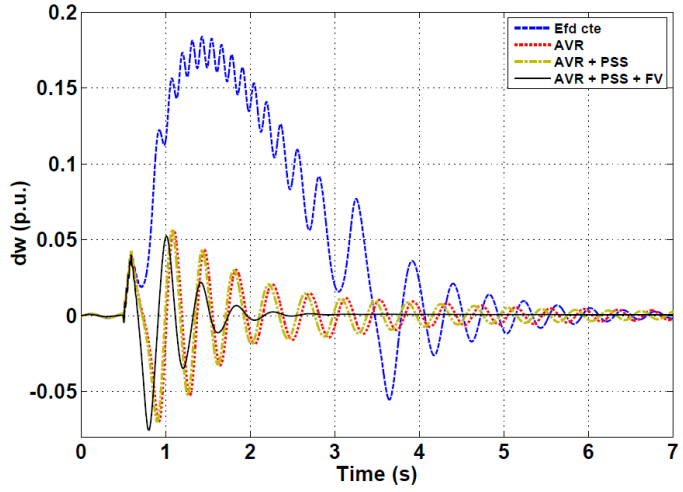


Fig. 18. Speed deviation for *FCT* at $t$ = 82,0926 *ms* with *Efd* constant

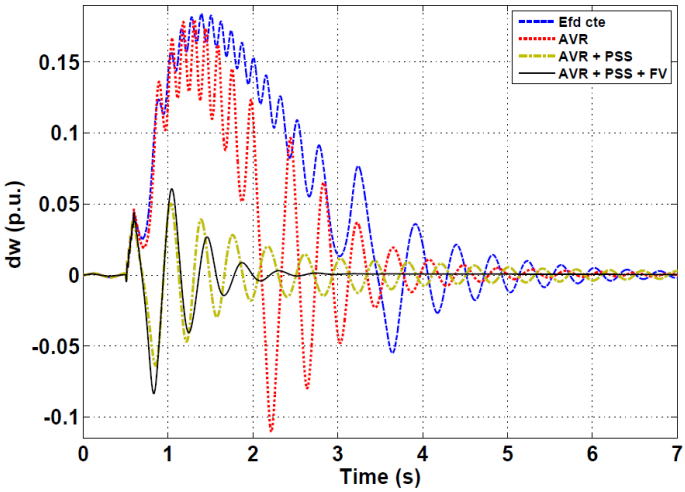


Fig. 19. Speed deviation for *FCT* at $t$ = 90,3614 *ms* with *AVR*

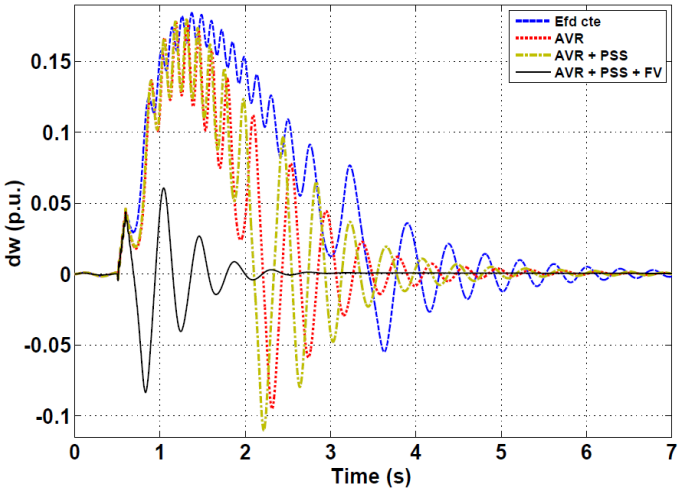


Fig. 20. Speed deviation for *FCT* at $t$ = 93,2946 *ms* with *AVR* and *PSS*

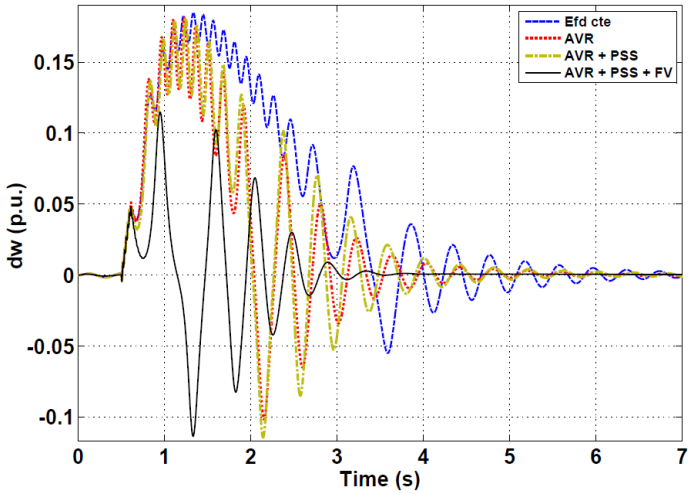


Fig. 21. Speed deviation for *FCT* at $t$ = 101,7191 *ms* with *AVR, PSS* and *FV*

## V. CONCLUSIONS

The assessment was highly satisfactory. Was proven to be *FV* an effective method to improve and enhance the stability margin in power systems. The results show a significant gain in transient stability of the system. It can sustain a larger value of *FCT* up 23.9079% (in order of 30ms) without losing synchronism as compared to uncontrolled system for the same fault.

Besides, *FV* works quite well like damper, reducing the settling times. It was shown in the $\Delta\omega$ and $P_a$ graphs as well the rotor angle swings.

After the *FV* effectiveness has been proven, this research invites to develop new proposals, including the assessment of the performance with parallel valves, which would help to improve the time-limiting valve action, training for all types of faults through neural networks and improve resilience and its adaptability, among others.

Other issues to consider are the negative influence that *FV* can have on the service life of the *ST* (valves, blades, pumps, and stages like the most important) and the potential impacts of the boiler, due to the sudden and strong changes in the steam pressure while the *FV* control is executing.

## REFERENCES


[1] I. Erlich, J. Löwen, J. M. Schmidt and W. Winter, "Advanced requirements for the thermal Power Plants for the stability in case of high wind power infeed" in *7th International Workshop on Large Scale Integration of Wind Power and on Transmission Networks for Offshore Wind Farm,* 2008, pp. 99.

[2] J. Machowski, A. Smolarczyk and J. W. Bialek, "Power System Transient Stability Enhancement by Co-ordinated Fast Valving and Excitation Control of Synchronous Generators", in *CIGRE Symposium "Working Plants and Systems Harder"*, 1999, pp. 200-06.

[3] F. B. Prioste, P. P. C. Mendes and C. Ferreira, "Power System Stability Enhancement by Fast Valving", in *Transmission & Distribution Conference & Exposition: Latin America, IEEE/PES*, 2004.

[4] P. Kundur, Ed. 1994. "*Power System Stability and Control"*, McGraw-Hill, Inc.

[5] IEEE Power System Engineering Committee, "A description of discrete supplementary controls for stability", in *IEEE Transmision Power Appar. Systems*, 1978, PAS-97, (1), pp. 149-157.

[6] R. Patel, and K. Pagalthivarthi, "Artificial Neural Network based Turbine Fast Valving for Enhancement of Power System Transient Stability", *Journal of Electrical Engineering*, Vol. 57, No. 1, p.p. 3–11.

[7] R. Patel, T. S. Bhatti and D. P. Kothari, "Improvement of Power Systems transient stability by coordinated operation of fast valving and breaking resistor", *IEEE Proc-Generation, Transmission and Distribution*, 2003, Vol. 150. No 3.

[8] F. J. Al-Azzawi and F. Omar, "Direct Approach to the Switching of Shunt Elements used for Multimachine Power System Transient Stability Augmentation", in *Proc. 5th Sci. Conference /SRC, Irak,* 1989, Vol. 6, Oct, p.p. 77–89.

[9] F. J. Al-Azzwi, N. M. Al-Wafi, A. K. Jassim and F. Omar, "Braking Resistor Size, Switching Instants and Assessment of Power System Transient Stability by Direct Methods", *Journal of Institution of Engineers (India)*, 1995, Nov, p.p. 175–180.

[10] IEEE committee report, "Recommended Practice for Excitation System Models for Power System Stability Studies", IEEE Standard 421.5-1992.

# ANNEX I: MODEL OF THE STEAM TURBINE

The *ST* is responsible of transforming the energy stored as steam pressure and temperature, thermal energy, into mechanical or rotational energy focused on its shaft. This energy is then transferred to the generator's rotor. This annex describes the operation of the *ST* and the steps taken in this research to adapt the basic model provided to MatLab for the purposes of the work.

## *I.I Physical description*

Normally, the *ST* consists of two or more sections coupled in series: *HP, IP* and *LP*. Depending on how the sections are arranged, the *ST* can be *tandem-compound* or *cross-compound*. In the first case, all sections are share the same shaft. The second case, by contrast, has two shafts connected to two generators controlled by one or more turbine sections [1].

For this research, we propose the use of a *ST tandem-compound* with single *RH* and its respective sections (*HP*, *IP*, *LP*), plus one *RH*. This is the type of mathematical model used by ALSTOM in their projects. Fig.AI.1 shows a scheme how will be made up the *ST*.

Generally, large turbines have at least four valves: Main inlet Stop Valves (*MSV*), *CV*, Reheated Stop Valves (*RSV*) and *IV*. The *MSV* and *RSV* are only used for emergency tripping, the *CV* and *IV* are used in controlling speed and load [1]. A crossover pipe (*CO*), carrying the steam between *IP* and *LP*, sections is also used.

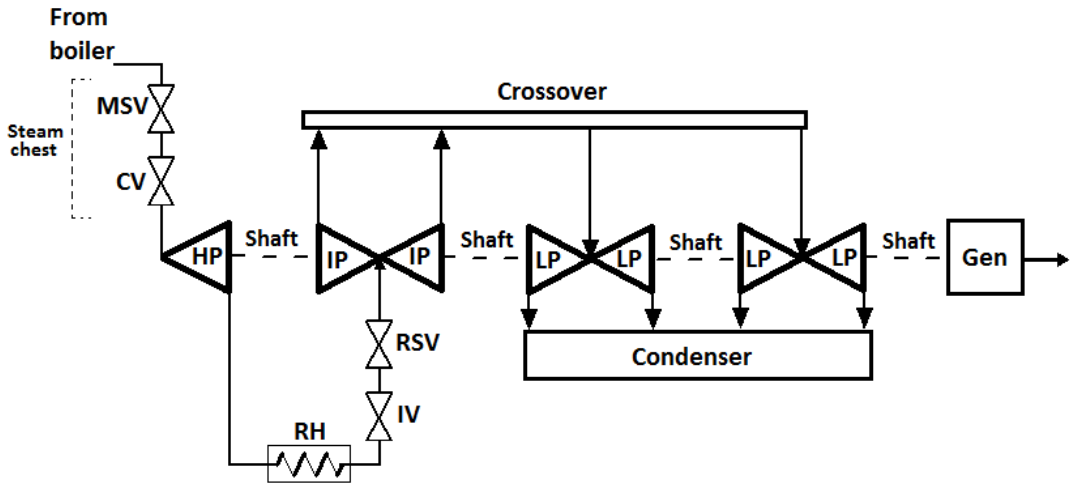


Fig.AI. 1. Scheme of tandem-compound *ST* with single *RH* configuration [1]

In abbreviated form, the main idea behind *ST* operation is to pass the steam generated by the boiler through each one of the sections. The steam passes from the boiler to the *HP* section, through the *MSV*, *CV* and the inlet pipe. The housing for the valves is called steam chest. A substantial amount of steam is stored in the chest and the inlet pipe to the *HP* section. This generates a steam delay. After the *HP* section, the exhaust steam is passed through the *RH*. The reheat steam flows into the *IP* section through the *IV* and the inlet pipe. Then, the exhaust steam from *IP* section to *LP* section passes through the *CO*. The waste steam is sent to the condenser to repeat the cycle. In each section, the steam is accelerated at high speed on the blades and the kinetic energy of the high velocity of the steam is converted into torque by the moving blades, resulting in movement of the turbine shaft. The movement generates a mechanical torque ($T_m$), which is converted to $P_m$.

## *I.II Mathematical model of ST*

A generic mathematical model of a *ST* is based on the study of the transfer functions of the different sections and their contributions to the total $T_m$.

The time constants of each turbine stage, $T_i$, may be obtained using a simple model of steam flow through a steam vessel, as shown in Fig. AI.2. The vessel introduces a time delay: the changes in the steam flow at the input take a finite time to appear in the output. This time delay can be quantified by considering a steam vessel of volume *V*, which stores a mass of steam *m* at a steam pressure. $Q_{in}$ and $Q_{out}$ are the steam mass flow rate at the input and output of the vessel respectively [2].

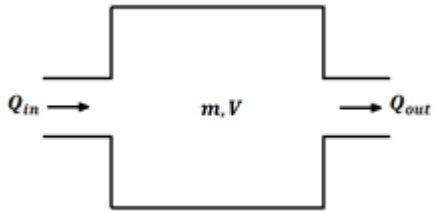


Fig.AI. 2. Steam Vessel Model

The continuity equation for the vessel is

$$\frac{dW}{dt} = V\frac{d\rho}{dt} = Q_{in} - Q_{out} \qquad (Eq.AI.1)$$

Where *W* is the weight of the steam in the vessel [kg] and $\rho$ is the density of steam [kg/m$^3$].

Assuming $Q_{out}$ to be proportional to pressure of steam in the vessel, *P*

$$Q_{out} = \frac{Q_0}{P_0}P \qquad (Eq.AI.2)$$

With $P_o$ being the rated pressure and $Q_o$ the rated output of the vessel.

When $Q_{in}$ changes due to the motion of the valve and its change in position, $\rho$ changes at a rate proportional to the difference between $Q_{in}$ and $Q_{out}$. If the steam temperature is considered constant, the change of $\rho$ must result in a pressure change as:

$$Q_{in} - Q_{out} = V\frac{\partial \rho}{\partial P}\frac{dP}{dt} = V\frac{\partial \rho}{\partial P}\frac{P_0}{Q_0}\frac{dQ_{out}}{dt} = T_v\frac{dQ_{out}}{dt}, \text{where } T_v = \frac{P_0}{Q_0}V\frac{\partial \rho}{\partial P} \quad (Eq.AI.3)$$

The transfer function of steam in the container is obtained by applying the Laplace transform. Here, $T$ is the time delay imposed by the vessel, which is directly proportional to the steam vessel volume. Then:

$$Q_{in} - Q_{out} = T_v s Q_{out} \qquad or \qquad \frac{Q_{out}}{Q_{in}} = \frac{1}{1 + T_v s} \qquad (Eq.AI.4)$$

As we stated before, the force on each rotor blade, and therefore the $T_m$ of the *ST*, is proportional to *Q*

$$T_m = kQ \qquad (Eq.AI.5)$$

Where *k* is constant.

As the *CV* opens, there is a change in the steam flow. This introduces a time constant in the chest ($T_{CH}$), due to the charging time of the steam chest and inlet piping to the *HP* section. The *RH* holds a substantial amount of steam and the time constant associated is $T_{RH.}$ The representation of the *RH* differs slightly because it assumes a restriction to the flow by the *IV*, then the *RH* pressure will be the integral of the net flow into the *RH* [3].

The *IP* section and inlet pipe have a time constant, $T_{IP}$, allowing computation of pressure drop of the *IV*. The steam flow into the *LP* sections experiences an additional time delay associated with the *CO* piping and this is called $T_{CO}$.

Finally, the model used to describe the *ST* behavior is shown in Fig. AI.3.

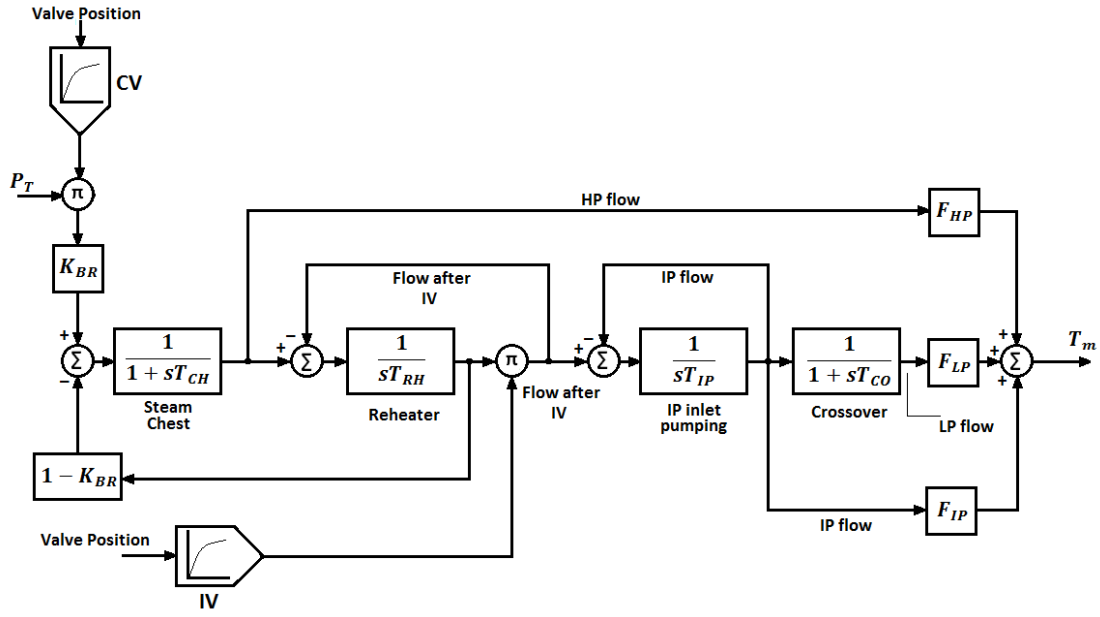


Fig.AI. 3. Steam Turbine model

This model also has a negative feedback loop of the reheat pressure to the *HP* section, and accounts for the reduction in pressure difference across the section when the *RH* pressure is high. This guarantees a safe operation of the valve.

The coefficients $F_{HP}$, $F_{IP}$ and $F_{LP}$ represent the contributions from *HP*, *IP* and *LP* turbine sections respectively to $P_m$. The sum of all contribution gives the total mechanical torque $T_m$ generated by the *ST*.

### *I.III Implementation of ST in MatLab/Simulink and SimPowerSystems toolbox*

The *ST* block set in *SimPowerSystems* is called *"Steam Turbine and Governor"*. It implements a complete tandem-compound steam prime mover, including a speed

governing system, a four-stage *ST* and a shaft with up to four masses. The default model of the *ST* is shown in Fig. AI.4.

The *ST* has four stages, each modeled by a first-order transfer function. The first stage represents the steam chest while the three other stages represent either *RH* or *CO* piping. Fractions F2 to F5 are used to distribute the turbine power to the various shaft stages.

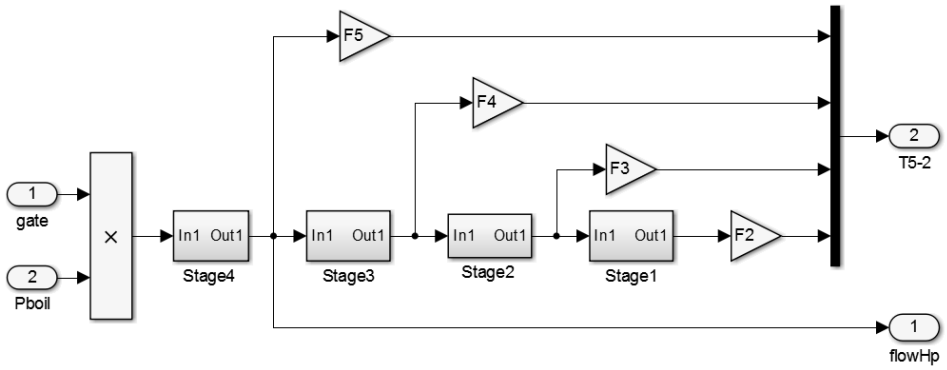


Fig.AI. 4. Default model of *ST* implemented by *SimPowerSystems* toolbox

As can be seen, this model does not contain the *IV*, needed to carry out the *FV* relevant study and therefore it is necessary to make some modifications to achieve the similarity to the theoretical model shown in Fig. AI.3. The final model is presented in the Fig. AI.5.

The speed governing system consists of a proportional regulator, a speed relay, and a servomotor controlling the gate opening. This model is proposed in [2] and is shown in Fig AI.6.

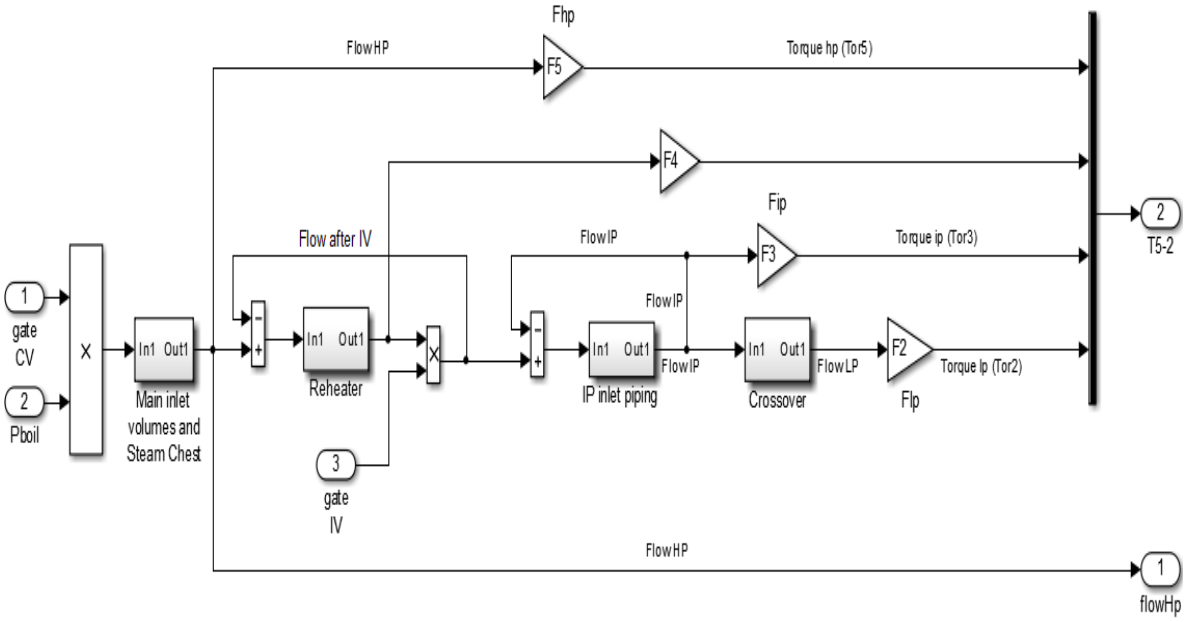


Fig.AI. 5. Customized model of tandem-compound *ST* with single *RH* implemented in *SimPowerSystems*

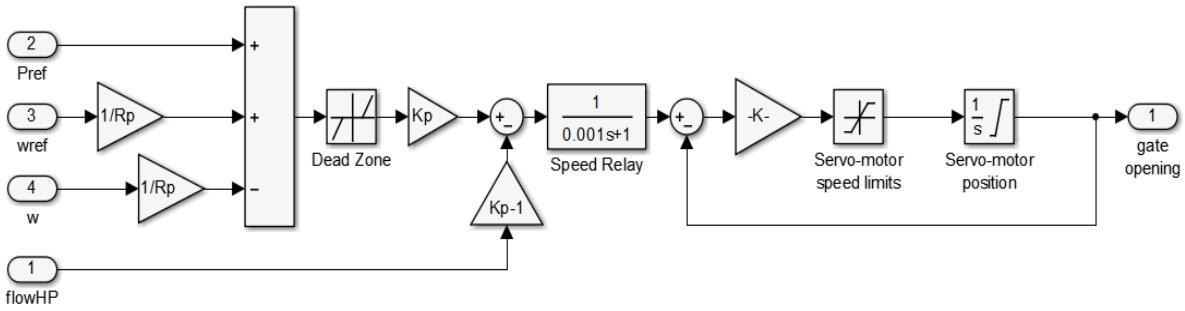


Fig.AI. 6. Default model of speed governor implemented in *SimPowerSystems*

This default model must also be modified because it only has one servomotor to one gate or valve. In this case, only the *CV* has one, but we need two independent servomotors to control both valves, the *CV* and *IV*. Another required change is in the characteristic curves of the valves. The default model shows a linear behavior of the strokes versus steam flow through the valves. In practice, the valves have a special non-linear behavior, depending of the valve type. This behavior is shown in

Fig.AI.7 and Fig.AI.8 for the characteristic curves of *CV* and *IV* respectively. Figure AI.9. shows the final, customized model for the *CV* and *IV* servomotors.

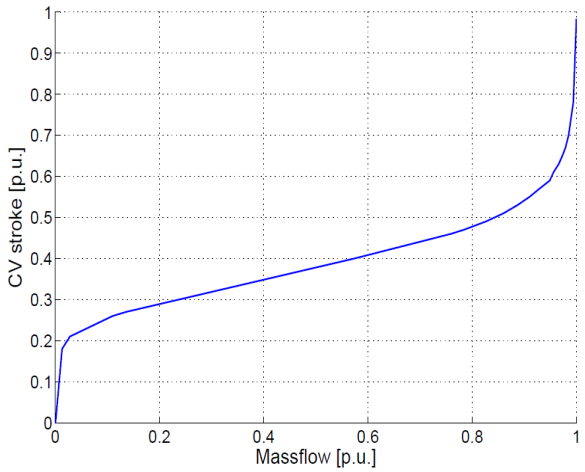


Fig.AI. 7. *CV* stroke vs. Flow characteristic curve

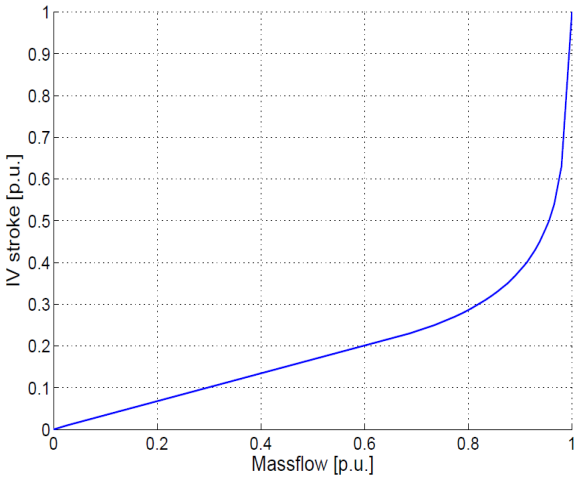


Fig.AI. 8. *IV* stroke vs. Flow characteristic curve

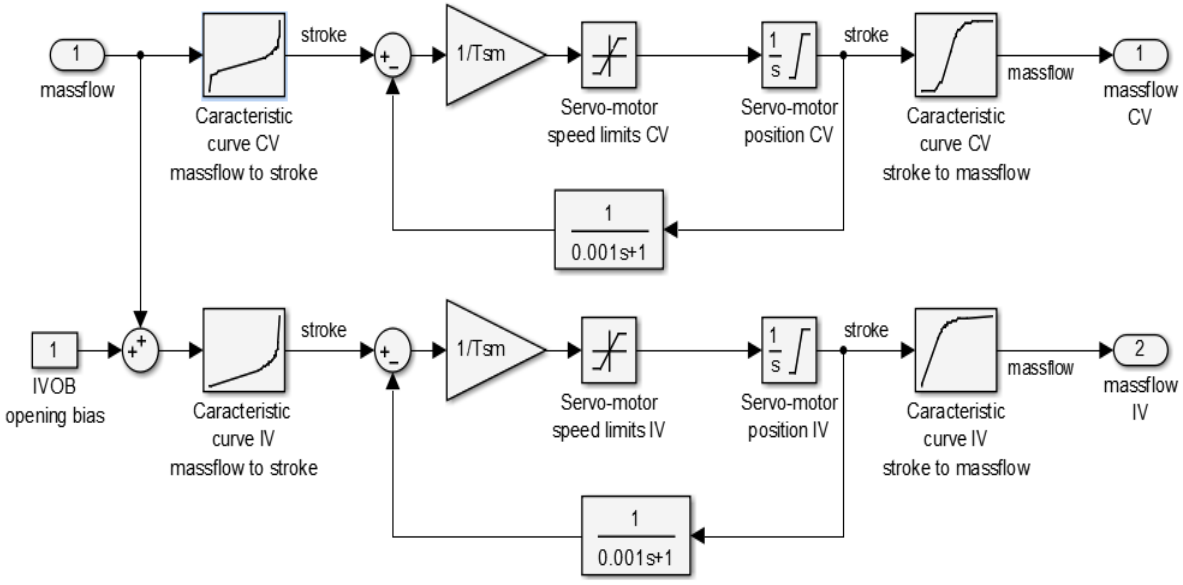


Fig.AI. 9. Model of servomotors customized for *CV* and *IV*

## ANNEX II: THEORY OF SYNCHRONOUS MACHINES

### *II.I Physical description*

Synchronous *Gen* is the main source of electric energy in power systems. It is the element which transforms the mechanical energy from the rotor or $T_m$ to electric energy in its terminals, $T_e$ or $P_e$.

Physically, the machine consists of two essential elements: Rotor and Stator. The field and the armature are located in the rotor and stator, respectively. This is shown in Fig.AII.1. The field winding carries direct current and produces a magnetic field which induces alternating voltage in the armature windings. The three-phase windings of the armature are distributed 120° apart in “space”. Then, the uniform rotation of the magnetic field produces voltages displaced by 120° in “time” phase in the windings [1].

The armature produces a magnetic field in the air-gap rotating at synchronous speed. The field produced by the direct current in the rotor winding, on the other hand, revolves with the rotor. To generate a steady torque, the fields of the stator must rotate at the same speed. This is the reason why the rotor must run at the same speed, which is precisely the synchronous speed [1].

The synchronous speed depends of the number of field poles that the machine has and the frequency at which the machine works. It is given by

$$n = \frac{120f}{P_f} \qquad (Eq.AII.1)$$

Where $n$ is the speed in rev/min, $f$ is the frequency in Hz and $P_f$ is the number of field poles.

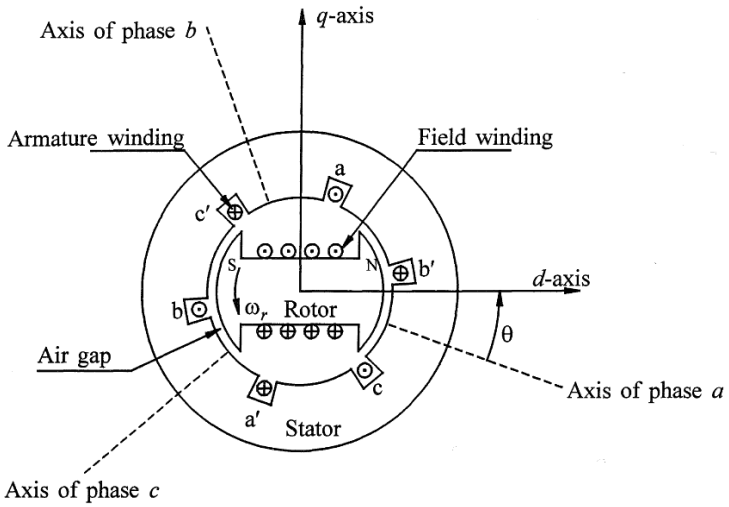


Fig.AII. 1. Schematic diagram of a three-phase synchronous machine [1]

The machines with more than one pair of field poles have stator windings made up of a corresponding multiple set of coils. Thus the angles are normally measured in electrical radians or degrees. The angle covered by one pair of poles is 2π electrical radians or 360 electrical degrees [1]. The relationship between angle $\theta$ in electrical units and the corresponding angle $\theta_m$ in mechanical units is

$$\theta = \frac{P_f}{2}\theta_m \qquad (Eq.AII.2)$$

Deriving Eq. AII.2 with respect to time, and using the mechanical units, we obtain for, a machine with $P_f$ field poles, the speed of rotation of the stator field as:

$$\omega_{sm} = \frac{2}{P_f}\omega_s \text{mech. rad/s or} \quad n_s = \frac{60\omega_{sm}}{2\pi} = \frac{120f}{P_f} \text{r/min} \qquad (Eq.AII.3)$$

Eq. AII.3 is the same as the synchronous speed of the rotor given by Eq. AII.1.

In Fig. AII.1 we can observe the direct axis (*d-axis*) and the quadrature axis (*q-axis*). In the figure, d-axis is centered magnetically in the center of the north pole and the *q-axis* is 90 electrical degrees ahead of the *d-axis*. The position of the rotor relative to the stator is measured by the angle $\theta$ between the d-axis and the magnetic axis of phase *a* winding [1].

In this case, *q-axis* is leading the *d-axis*, which selection is just arbitrary and based on the IEEE standard definition [4]. Alternatively, the *q-axis* could be chosen to lag the *d-axis* by 90 electrical degrees [5].

### *II.II Mathematical model of Synchronous Machine*

When a disturbance occurs in the power system, the changes in the armature and flux linkages create dynamic interactions in the synchronous machines. To understand the behavior of the machines under these conditions, it is necessary to adopt a mathematical model to quantify the changes in the currents and torques, representing the machine through a number of electrical circuits with resistors and self- and mutual-inductances [1].

When developing a complete model of a generator, the model is split into two sub-models: Mechanical (rotor acceleration equations of turbine-generator set) and Electric (electric flow dynamics of the *Gen*).

Any three-phase synchronous machine can be considered as a set of coupled electrical circuits, as shown in Fig. AII.2. The mathematical model we develop is based on the concept of a generalized or “ideal” synchronous machine with two poles (*q* and *d*). As mentioned before, the circuits considered here are:

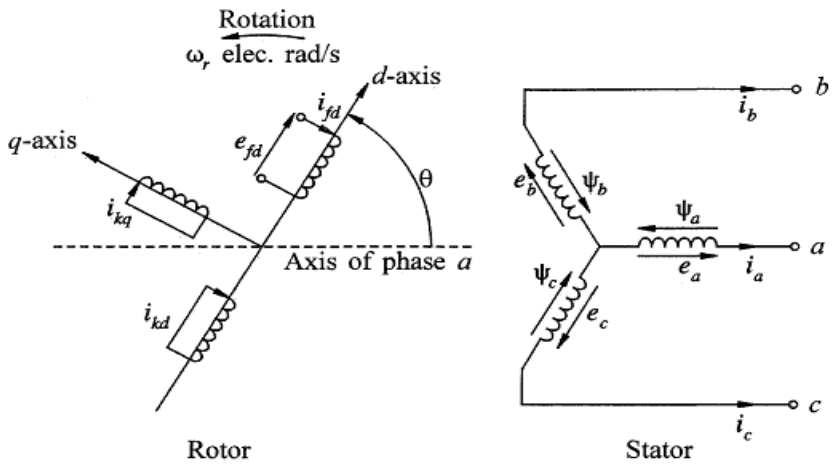


Fig.AII. 2. Ideal machine representation [1]

***Stator***: Composed by the three windings (*a, b, c*), each winding is represented by a resistor in series with an inductive reactance. They represents the copper losses of the winding conductor and the mutual inductance, respectively.

***Rotor***: It is where we found the *d-axis* and *q-axis*, composed by the field winding (*fd*) and three damper windings the *d-axis* amortisseur (*kd*), the two *q-axis* amortisseur (*kq1* and *kq2*), which are short-circuited.

Fig. AII.2 also shows the angle *θ* by which d-axis leads the magnetic axis of phase *a* winding and the rotor angular velocity $\omega_r$.

Sophisticated models generally require more data than we have, more time to develop the software to simulate it and more computational effort. Even if the rotor has only one physical winding, the model includes additional windings to consider the damper windings and the effect of the Eddy currents. Experience shows that, for stability studies, it is sufficient to use ideal models of one or two compensation windings in addition to the field winding [6].

In this research, we use the model recommended by the IEEE [7] for the generic synchronous machine. It has been already implemented in different software packages such as the *SimPowerSystems*[1] toolbox that works with MatLab/Simulink.

The equations associated with the stator circuits, together with the equations associated with the rotor circuits, contain inductance terms, which vary with the angle $\theta$ that in turn changes with time. This introduces considerable complexity in solving machine and power system problems. This research does not delve into the issue of time-varying equations. The interested reader is recommended to go to the references [1,7,8].

One way to solve this problem is to find a transformation that makes the equations independent of the position of the rotor. This is achieved by using the *qd0* transformation, also called *Park* transformation [1,9,10]. This procedure is based on the expression of the electrical stator and rotor quantities (linkages, voltages and currents), normally presented in the *abc* framework (three-phase), under reference rotor quantities, *d-axis* and *q-axis*. If this is achieved, the new quantities referenced in this framework do not depend on the position of the rotor, it would be rotating at the same speed [8].

The transformation should allow the inverse operation, which means convert any amount of the rotor to the stator framework. To do this, should be added to the *d* and *q* coordinates another parameter, the coordinate called *zero-sequence*, hence its name *dq0*.

The transformation from the *abc* phase variables or from the stator side to the *dq0* variables can be written in the following matrix form:

[1] The *SimPowerSystems* Toolbox starting to be one of the most useful and highly tools used by companies in the power market to make simulations and studies of power systems around the world.

$$\begin{bmatrix} v_d \\ v_q \\ v_0 \end{bmatrix} = \frac{2}{3}\begin{bmatrix} \cos\theta & \cos(\theta - 2\pi/3) & \cos(\theta + 2\pi/3) \\ -\sin\theta & -\sin(\theta - 2\pi/3) & -\sin(\theta + 2\pi/3) \\ 1/2 & 1/2 & 1/2 \end{bmatrix}\begin{bmatrix} v_a \\ v_b \\ v_c \end{bmatrix} \qquad (Eq.AII.4a)$$

The inverse transformation is given by

$$\begin{bmatrix} v_a \\ v_b \\ v_c \end{bmatrix} = \begin{bmatrix} \cos\theta & -\sin\theta & 1 \\ \cos(\theta - 2\pi/3) & -\sin(\theta - 2\pi/3) & 1 \\ \cos(\theta + 2\pi/3) & -\sin(\theta + 2\pi/3) & 1 \end{bmatrix}\begin{bmatrix} v_d \\ v_q \\ v_0 \end{bmatrix} \qquad Eq.AII.4b)$$

Another issue to consider is the per unit representation (p.u.). It is convenient to use it, since it normalizes the system's variables. Compared to the use of physical units, the p.u. system offers computational simplicity by eliminating units and expressing system quantities as dimensionless ratios. Thus, in the case of asynchronous machine, the p.u. system may be used to remove arbitrary constants and simplify mathematical equations so that they may be expressed in terms of equivalent circuits [1]. For these reasons is almost always used in the development of models of synchronous machines.

With this clarified, the next step is to resolve the electrical model of the synchronous machine. This electrical model is represented by a sixth-order state-space representation. It takes into account the dynamics of the stator, field and damper windings. The equivalent circuit of the model is represented in the rotor reference frame (*qd* frame). All rotor parameters and electrical quantities are viewed from the stator. They are identified by primed variables. The subscripts used are defined in table AII.I.

TABLE AII I
SUBSCRIPTS OF VARIABLES TO DESCRIBE THE SYNCHRONOUS MACHINE MODEL

| Subscripts | Meaning |
|---|---|
| *d, q* | d and q axis quantity |
| *R, s* | Rotor and stator quantity |
| *l, m* | Leakage and magnetizing inductance |
| *f, k* | Field and damper windingquantity |

The electrical model is shown in Fig. AII.3.

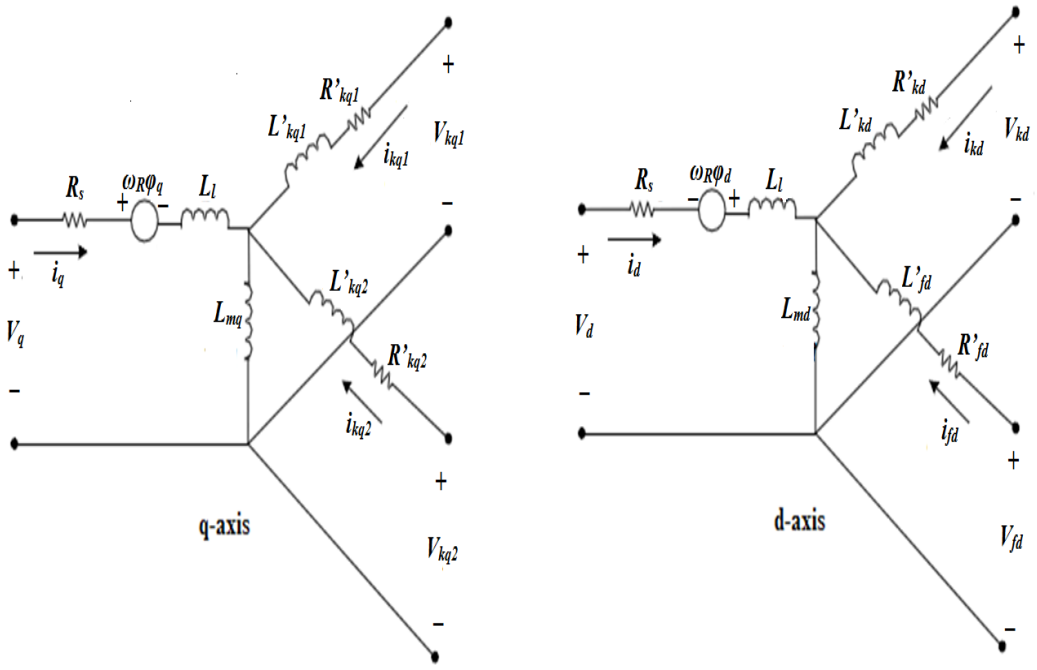


Fig.AII. 3. Electrical model of the synchronous machine

With the following equations:

$$V_d = R_s i_d + \frac{d\varphi_d}{dt} - \omega_R \varphi_q \quad (Eq.AII.5)$$

$$V_q = R_s i_q + \frac{d\varphi_q}{dt} + \omega_R \varphi_d \quad (Eq.AII.6)$$

$$V'_{fd} = R'_{fd} i'_{fd} + \frac{d\varphi'_{fd}}{dt} \quad (Eq.AII.7)$$

$$V'_{kd} = R'_{kd} i'_{kd} + \frac{d\varphi'_{kd}}{dt} \quad (Eq.AII.8)$$

$$V'_{kq1} = R'_{kq1} i'_{kq1} + \frac{d\varphi'_{kq1}}{dt} \quad (Eq.AII.9)$$

$$V'_{kq1} = R'_{kq1} i'_{kq1} + \frac{d\varphi'_{kq1}}{dt} \quad (Eq.AII.10)$$

$$\varphi_d = L_d i_d + L_{md}\left(i'_{fd} + i'_{kd}\right)(Eq.AII.11)$$

$$\varphi_q = L_q i_q + L_{mq} i'_{kq} \quad (Eq.AII.12)$$

$$\varphi'_{fd} = L'_{fd} i'_{fd} + L_{md}(i_d + i'_{kd})(Eq.AII.13)$$

$$\varphi'_{kd} = L'_{kd} i'_{kd} + L_{md}\left(i_d + i'_{fd}\right)(Eq.AII.14)$$

$$\varphi'_{kq1} = L'_{kq1} i'_{kq1} + L_{mq} i_q \quad (Eq.AII.15)$$

$$\varphi'_{kq2} = L'_{kq2} i'_{kq2} + L_{mq} i_q \quad (Eq.AII.16)$$

In the electrical part, $T_e$ is calculated, as well as the active and reactive power at the terminals given by the following equations

$$T_e = \varphi_d i_q - \varphi_q i_d \quad (Eq.AII.17)$$

$$P_t = \varphi_d i_d + \varphi_q i_q \quad (Eq.AII.18)$$

$$Q_t = \varphi_q i_d - \varphi_d i_q \quad (Eq.AII.19)$$

The mechanical model is based on the equations of motion. These equations are of main importance in power system stability analysis, because the rotational inertia equations describe the effect of unbalance between the $T_e$ and the $T_m$ of the individual machines.

When an unbalance between the torques acting on the rotor occurs, an acceleration or deceleration torque appears. It is given by:

$$T_a = T_m - T_e \quad (Eq.AII.20)$$

The combined inertia of the generator and prime mover is accelerated by the unbalance in the applied torques. Hence, the equation of motion is

$$J\frac{d\omega_m}{dt} = T_a = T_m - T_e \qquad (Eq.AII.21)$$

Where *J* is the combined moment of inertia of *Gen* and turbine [kg/m$^2$] and $\omega_m$ is angular velocity of the rotor [mech. rad/s].

The moment of inertia *J* in terms of p.u. inertia constant *H* is

$$J = \frac{2H}{\omega_{0m}^2} VA_{base} \qquad (Eq.AII.22)$$

Substituting the above in Eq.AII.21 and observing that $T_{base} = VA_{base}/\omega_{0m}$, the equation of motion p.u. form is

$$2H\frac{d\overline{\omega_r}}{dt} = \overline{T_m} - \overline{T_e}\,, \qquad \text{where } \overline{\omega_r} = \omega_r/\omega_0 \qquad (Eq.AII.23)$$

Where, $\omega_r$ is the angular speed of the rotor [electrical rad/s] and $\omega_0$ is its rated value.

If $\delta$ is the angular position of the rotor in electrical radians with respect to asynchronously rotating reference and $\delta_0$ is its value at t=0, then

$$\delta = \omega_r t - \omega_0 t + \delta_0 \qquad (Eq.AII.24)$$

Taking the time derivative,

$$\frac{d\delta}{dt} = \omega_r - \omega_0 = \Delta\omega_r \qquad (Eq.AII.25)$$

Where $\Delta\omega_r$ is the speed deviation. Differentiating again

$$\frac{d^2\delta}{dt^2} = \frac{d\omega_r}{dt} = \frac{d(\Delta\omega_r)}{dt} \qquad (Eq.AII.26)$$

Substituting $d\overline{\omega_r}/dt$ given by Eq.AII.26 in Eq.AII.23 and including a component of damping torque,

$$\frac{2H}{\omega_0}\frac{d^2\delta}{dt^2} = \overline{T_m} - \overline{T_e} - K_D\Delta\overline{\omega_r} \qquad (Eq.AII.27)$$

Where $K_D$ is a damping constant and

$$\Delta\overline{\omega_r} = \frac{\Delta\omega_r}{\omega_0} = \frac{1}{\omega_0}\frac{d\delta}{dt} \qquad (Eq.AII.28)$$

It is clear that the Eq.AII.27 is the same "*swing equation*" or "*backswing equation*" as was shown in the paper in the Eq. (1).

The mechanical starting time ($T_M$) is the time required for rate torque to accelerate the rotor from standstill to rated speed. Is given by

$$T_M = 2H \qquad (Eq.AII.29)$$

For the analysis of power system dynamic performance, the component models are expressed in the state-space form or the block diagram form. The state-space form requires the component models to be expressed as a set of first order differential equations [1]. The swing equation Eq.AII.27, expressed as two first order differential equations, becomes

$$\frac{d\overline{\omega_r}}{dt} = \frac{1}{2H}(\overline{T_m} - \overline{T_e} - K_D\Delta\overline{\omega_r}) \qquad (Eq.AII.30)$$

$$\frac{d\delta}{dt} = \omega_0 \Delta\overline{\omega_r} \qquad (Eq.AII.31)$$

### *II.III Steady-state analysis*

For stability analysis, it is necessary to find the initial steady-state values of the machine variables as a function of specified terminal quantities. To simplify the steady state analysis, the equations are developed using phasor representation. The *dq* components of armature voltage are scalar quantities, thus these quantities could be expressed in a complex plane having *d*-and *q-axes* as coordinates.

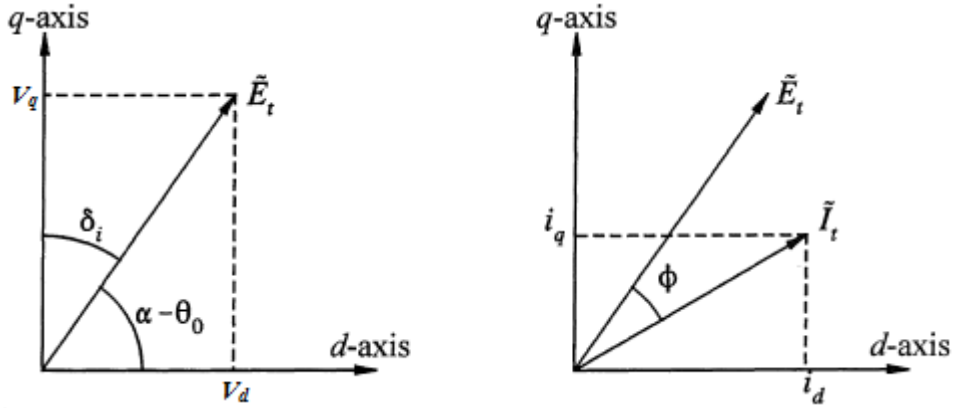


Fig.AII. 4. Representation of dq components of armature voltage and currents as phasors [1]

This is illustrated in Fig. AII.4 and it is conceptually similar to phasor representation of alternating quantities varying sinusoidally with respect to the time. Thus, the armature terminal voltage ($E_t$) could be expressed in complex form as

$$\widetilde{E_t} = V_d + jV_q \qquad (Eq.AII.32)$$

Calling $\delta_i$ the angle by which the *q-axis* leads the phasor *Et* at *t* = 0,

$$V_d = E_t \sin \delta_i \qquad (Eq.AII.33)$$

$$V_q = E_t \cos \delta_i \qquad (Eq.AII.34)$$

Similarly for the armature terminal current ($I_t$), if $\phi$ is the power factor angle, then

$$i_d = I_t \sin(\delta_i + \emptyset) \qquad (Eq.AII.35)$$

$$i_q = I_t \cos(\delta_i + \emptyset) \qquad (Eq.AII.36)$$

$$\widetilde{I_t} = i_d + j i_q \qquad (Eq.AII.37)$$

With the relationships between *dq* components of $E_t$ and $I_t$ and from Eq.AII.5 and Eq.AII.6,

$$V_d = -\omega_r \varphi_q - R_s i_d = \omega_r L_q i_q - R_s i_d = X_q i_q - R_s i_d \qquad (Eq.AII.38)$$

$$V_q = \omega_r \varphi_d - R_s i_q = -X_d i_d + X_{md} i_{fd} - R_s i_q \qquad (Eq.AII.39)$$

Where the reactances $X_d$ and $X_q$ are the *d*- and *q-axis* synchronous reactances, respectively. They represent the inductive effects of the armature *mmf* wave by separately accounting for its *d*- and *q-axis* components.

To identify the *d*- and *q-axis* positions relative to $E_t$, could be define a voltage $E_q$ as

$$\widetilde{E_q} = \widetilde{E_t} + (R_s + jX_q)\widetilde{I_t} = j\left[X_{md} i_{fd} - (X_d - X_q) i_d\right] \qquad (Eq.AII.40)$$

For the steady state, the terminal active and reactive powers, $P_t$ and $Q_t$ respectively, have the same equations shown in Eq.AII.18 and Eq.AII.19 just changing the flux for the *d*- and *q-axes* voltages.

For the $T_e$ and based on Eq.AII.17, could be writing in terminal terms as

$$T_e = P_t + R_s I_t^2 \qquad (Eq.AII.41)$$

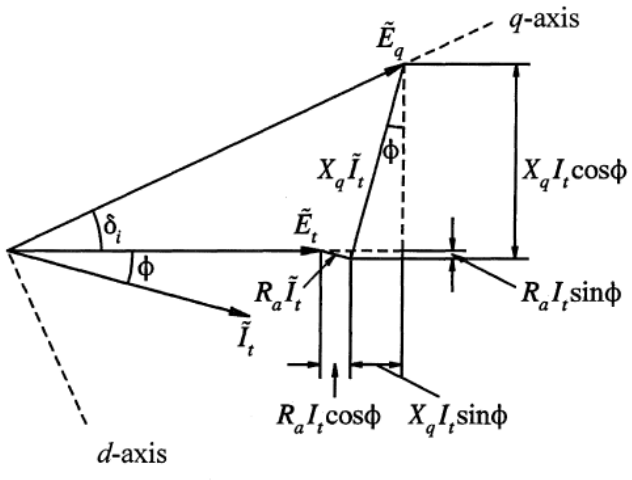


Fig.AII. 5. Steady state phasor diagram [1]

Since $E_q$ lies along the *q-axis*, as is illustrated in Fig. AII.5, the initial internal angle is given by

$$\delta_i = \tan^{-1}\left(\frac{X_q I_t \cos\emptyset - R_s I_t \sin\emptyset}{E_t + R_s I_t \cos\emptyset + X_q I_t \sin\emptyset}\right) \qquad (Eq.AII.42)$$

To compute all values to establish the steady state, normally, $P_t$, $Q_t$, and magnitude of $E_t$ are specified. The corresponding $I_t$ and $\phi$ are

$$I_t = \frac{\sqrt{P_t^2 + Q_t^2}}{E_t} \qquad (Eq.AII.43)$$

$$\emptyset = \cos^{-1}\left(\frac{P_t}{E_t I_t}\right) \qquad Eq.AII.44)$$

Thus, using the equations Eq.AII.32 to Eq.AII.44, the other equations are written as

$$\varphi_d = V_q + R_s i_q \qquad (Eq.AII.45) \qquad \varphi_q = -V_d - R_s i_d \qquad (Eq.AII.46)$$

$$V_{fd} = R_{fd} i_{fd} \qquad (Eq.AII.47)$$

$$i_{fd} = \frac{V_q + R_s i_q + X_d i_d}{X_{md}} \qquad (Eq.AII.48)$$

$$\varphi_{fd} = \left(L_{md} + L_{fd}\right) i_{fd} - L_{md} i_d \qquad (Eq.AII.49)$$

$$\varphi_{kd} = L_{md}\left(i_{fd} - i_d\right) \qquad (Eq.AII.50)$$

$$\varphi_{kq1} = \varphi_{kq1} = -L_{mq} i_q \qquad (Eq.AII.51)$$

## *II.IV Implementation of Synchronous Machines in MatLab/Simulink and SimPowerSystems toolbox*

In this research was developed one model of the synchronous machine basing on the whole set of equations presented in the above section. The model was implemented using MatLab/Simulink.

The blocks used to model the machine are shown below

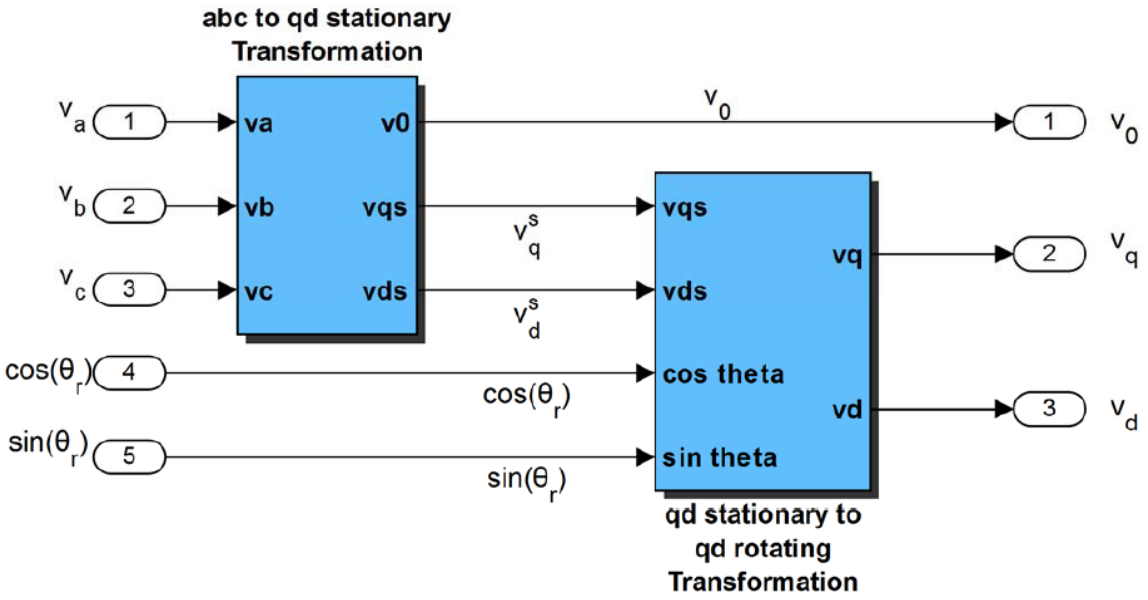


Fig.AII. 6. Transformation from *abc* frame to *qd rotating* frame applying Eq.AII.4b.

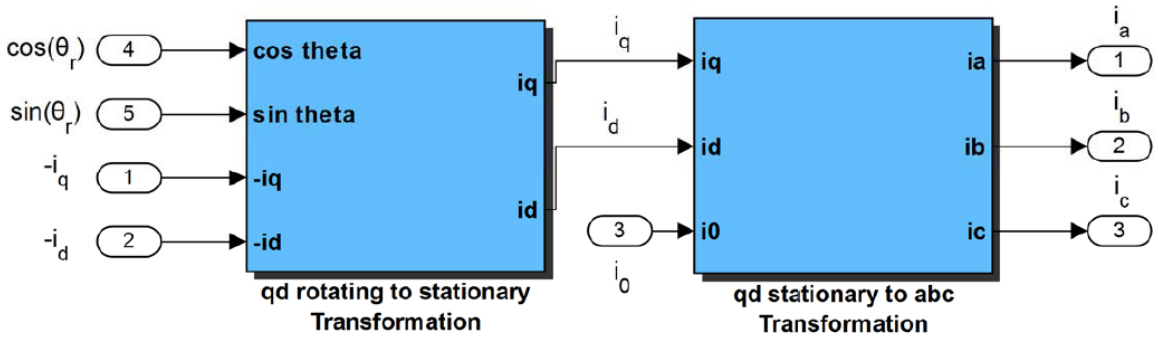


Fig.AII. 7. Transformation from *qd rotating* frame to *abc* frame applying Eq.AII.4a.

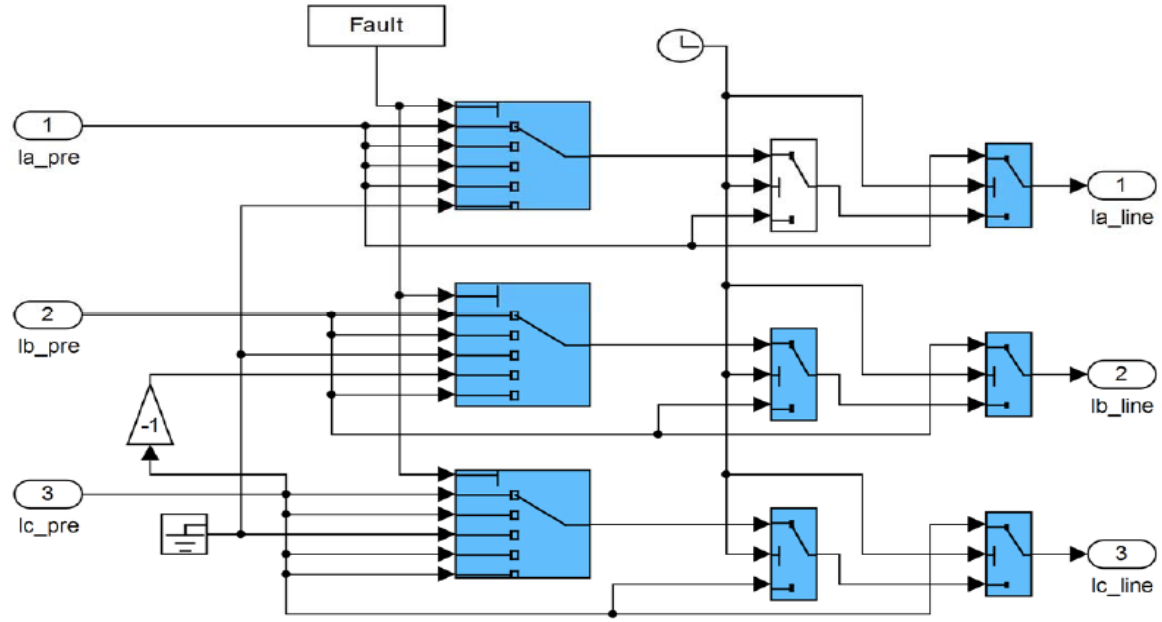


Fig.AII. 8. Block to create the current faults.

It is important to notice that the currents on the *abc* frame are the currents to which the faults or disturb are applied.

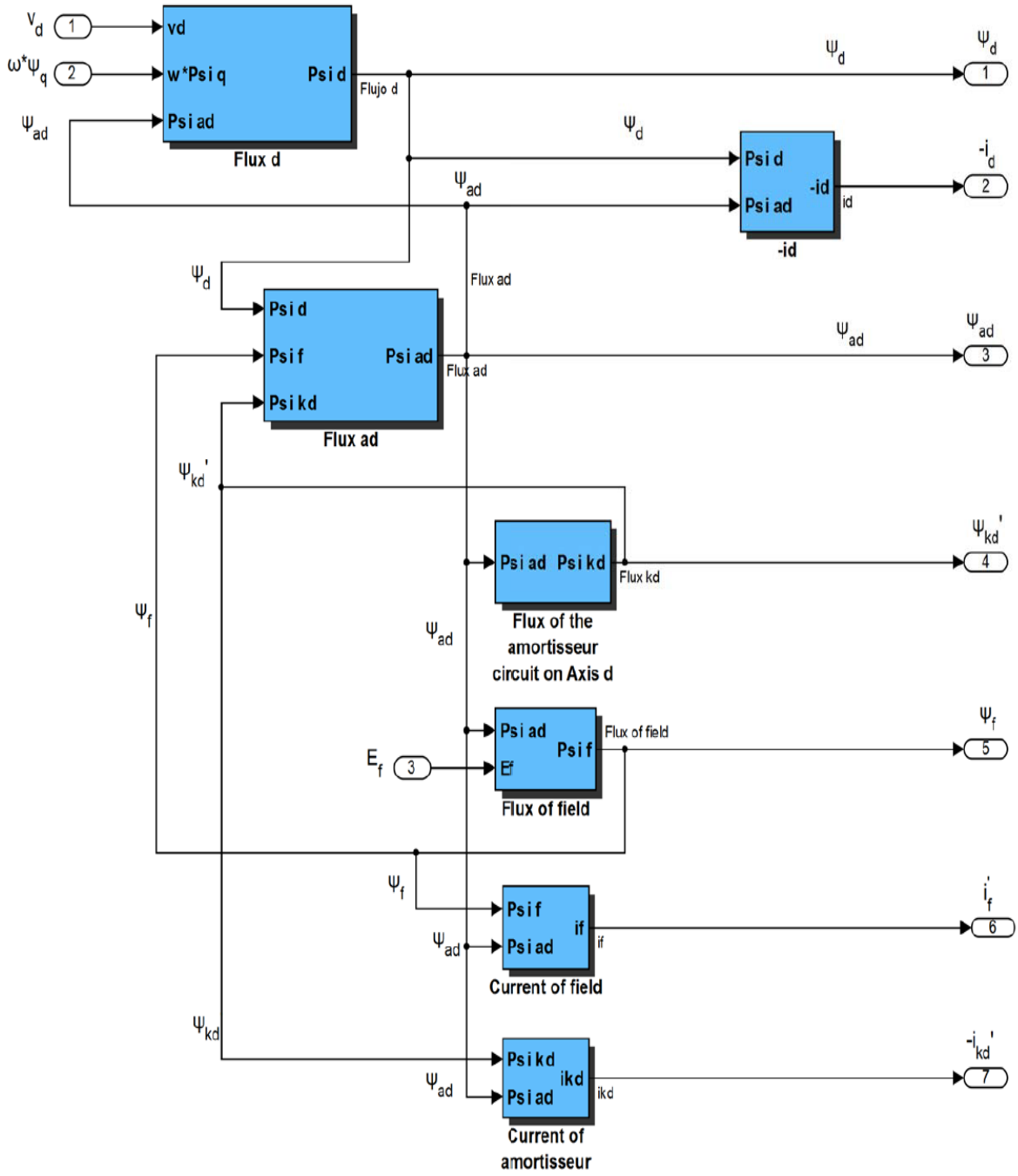


Fig.AII. 9. D-axis equations diagram blocks

The equations used to resolve these blocks were Eq.AII.5, Eq.AII.7, Eq.AII.8, Eq.AII.11, Eq.AII.13 and Eq.AII.14.

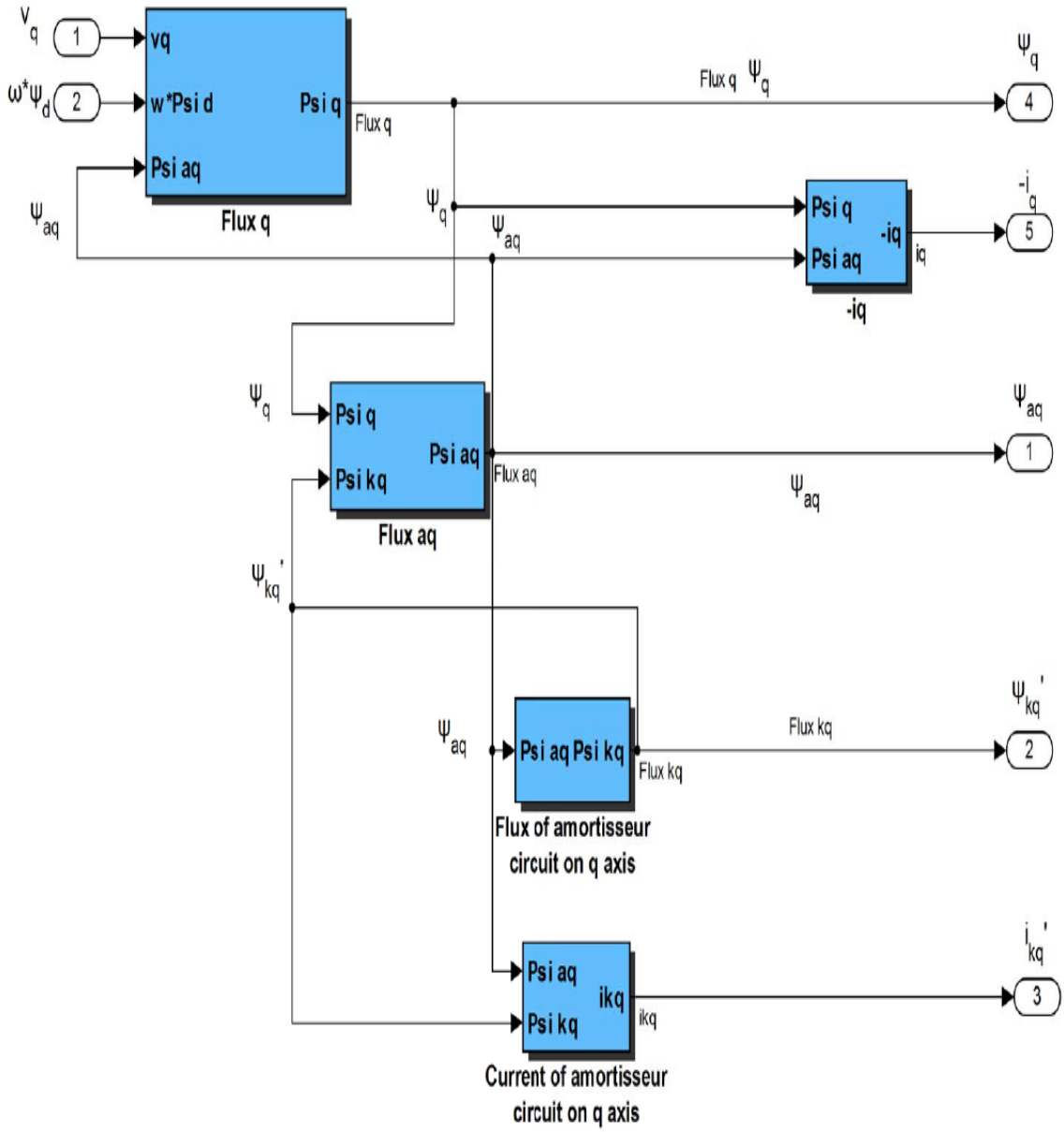


Fig.AII. 10. Q-axis equations diagram blocks

The equations used to resolve these blocks were Eq.AII.6, Eq.AII.9, Eq.AII.10, Eq.AII.12, Eq.AII.16 and Eq.AII.15

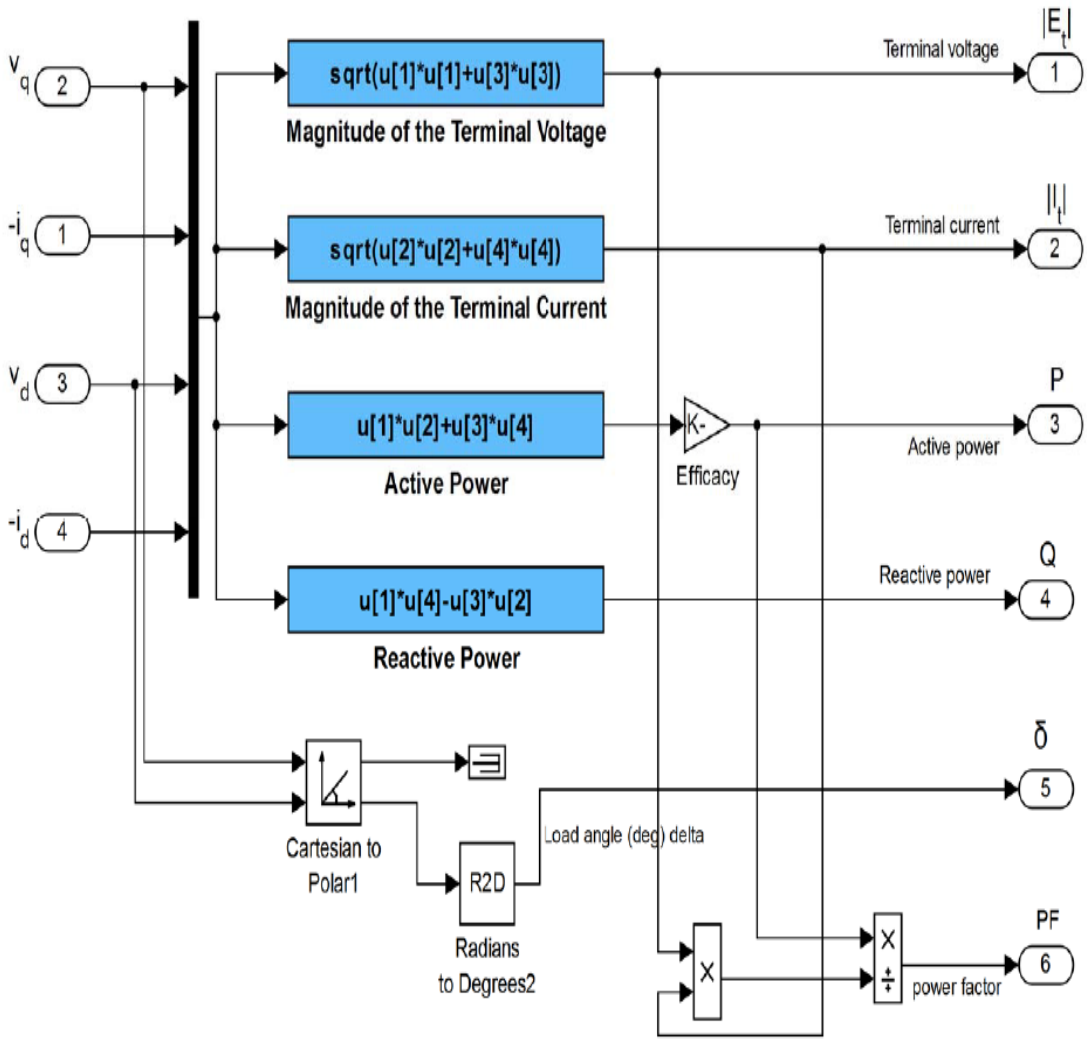


Fig.AII. 11. Electrical equations diagram blocks

The equations used to describe the electrical behavior of the synchronous machine were Eq.AII.18, Eq.AII.19, Eq.AII.44 and the magnitudes for the phasors from the Eq.AII.32 and Eq.AII.37

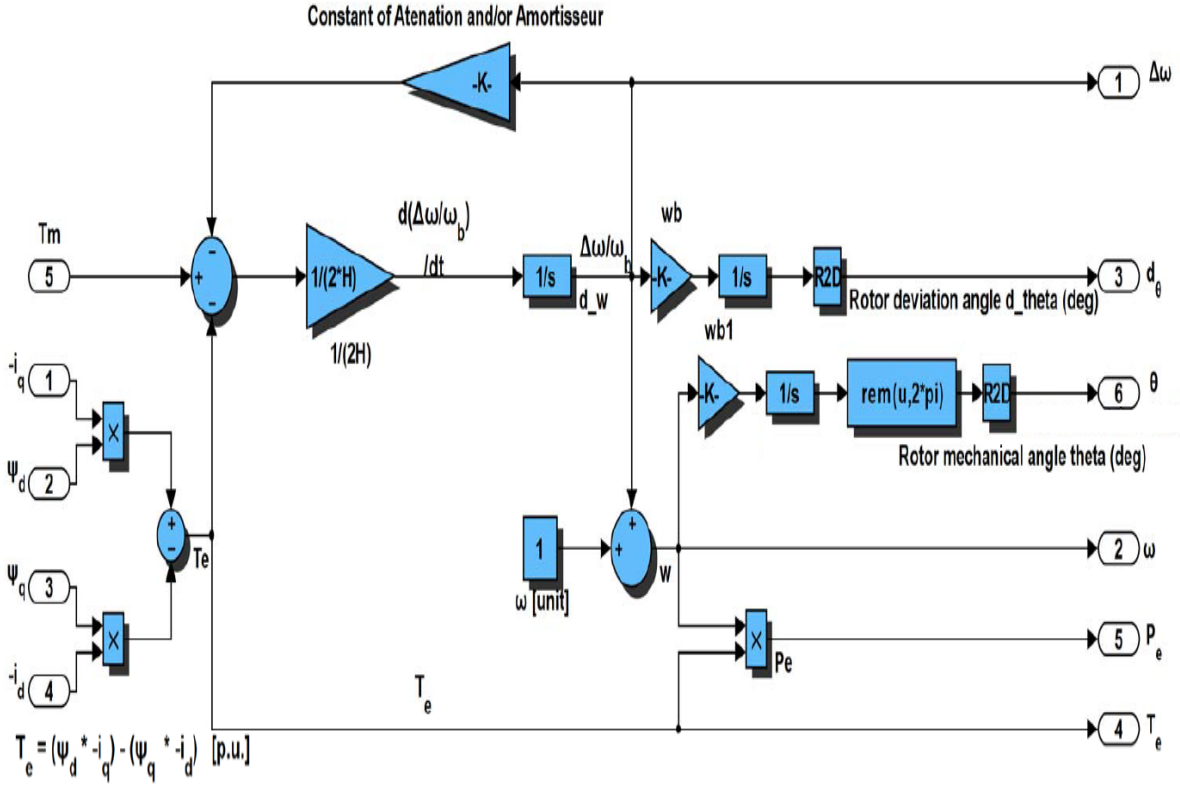


Fig.AII. 12. Mechanical equations diagram blocks

The equations used to describe the mechanical behavior of the synchronous machine, $P_e$ and $T_e$ were Eq.AII.17, Eq.AII.24, Eq.AII.25, Eq.AII.26, Eq.AII.27, Eq.AII.28, Eq.AII.30 and Eq.AII.31

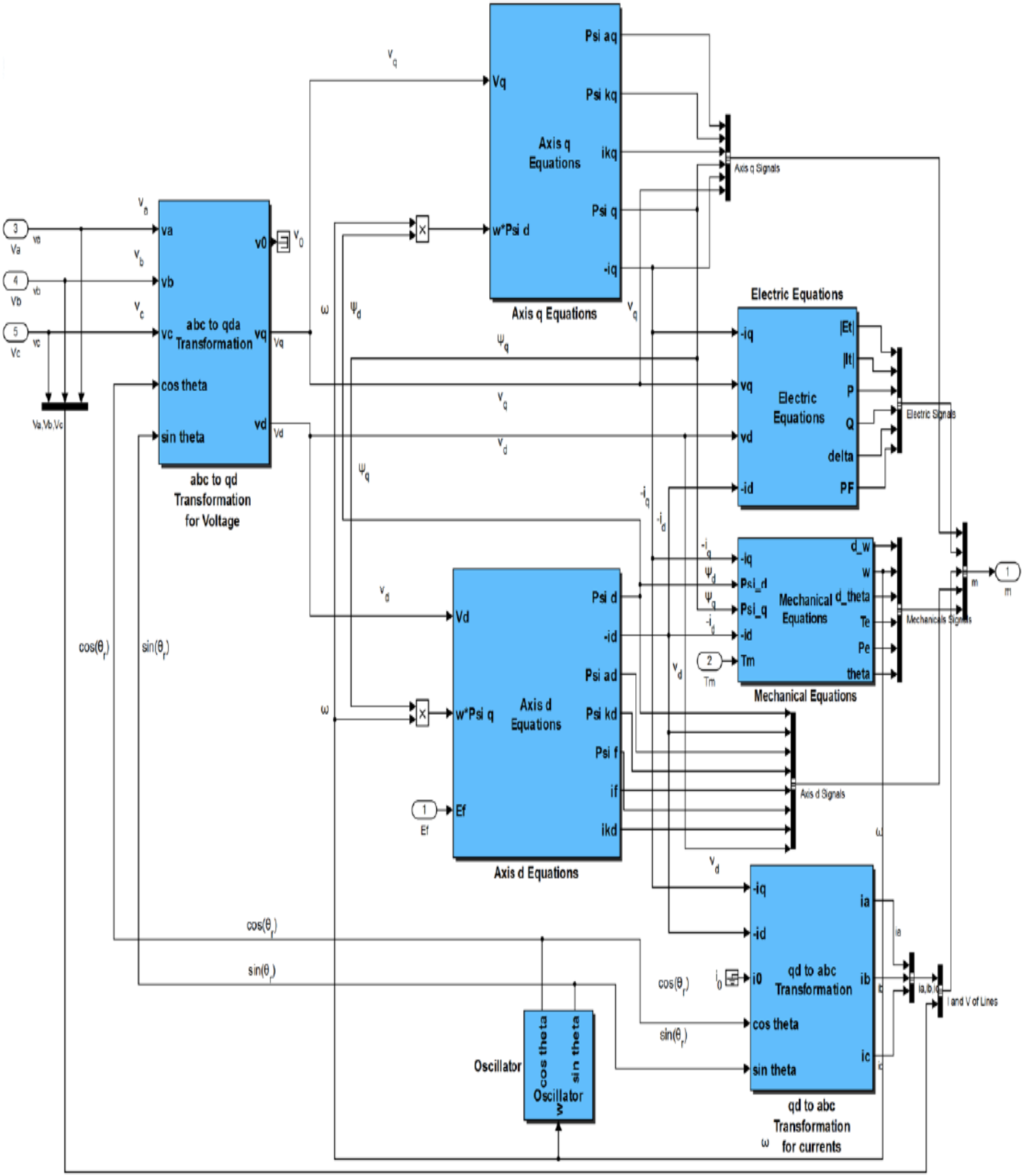


Fig.AII. 13. Complete system block diagram of the synchronous machine

The synchronous machine model works together with an infinite bus, which is comprised of a voltage generator per phase, a voltage fault simulation to introduce different kinds of faults to the grid and the kind of net with the strong coefficient of power network, all shown in the Fig AII.14.

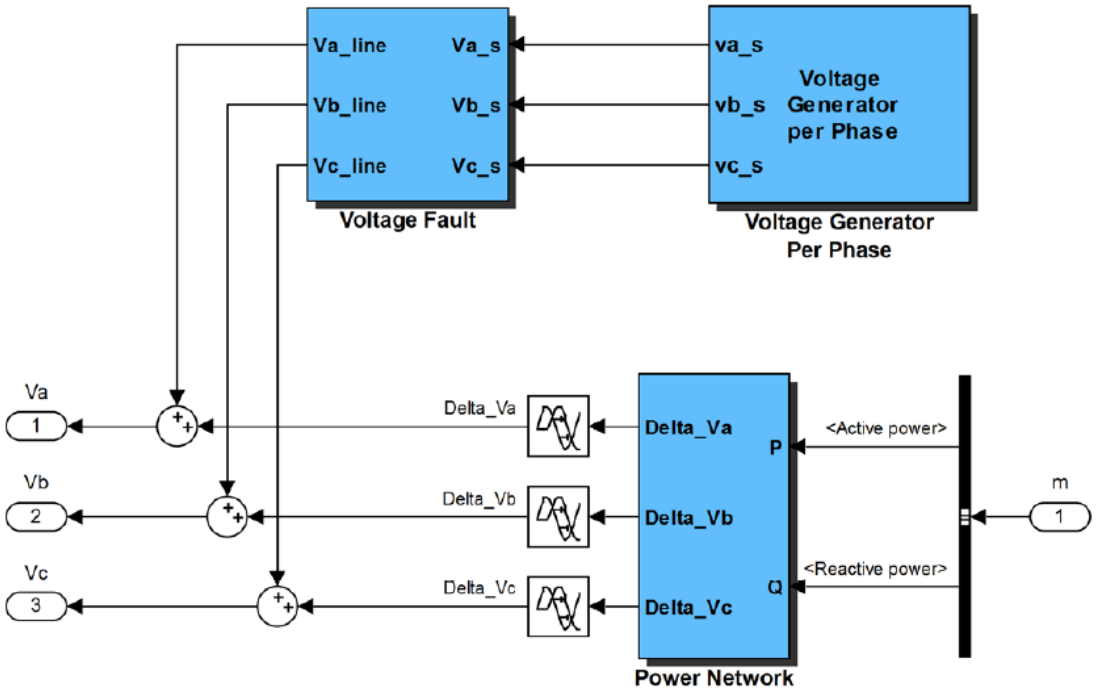


Fig.AII. 14. Block diagram of infinite bus

The voltage generator principle is generate a sine wave with an amplitude defined and time-varying angle equal $2\pi\omega t$ for the phase *a*. Phases *b* and *c* are out of phase by -2π/3 and 2π/3 radians, respectively.

The voltage faults are the same system as the current faults shown in Fig. AII.8.

In the power network box, we found the correlation between the type of network that is simulated (weak, medium and strong), the ratio between the resistance and reactance of the lines, the short circuit power of it and the active and reactive deltas generated by the fault on the net.

The power system is represented by a three-phase source block with balanced three-phase voltage source and internal *R-L* impedance or its ratio. These three voltage sources are connected in *Y* with a neutral connection that can be internally grounded or made accessible. The source's internal resistance and inductance can be specified by entering the source inductive short-circuit level and *X/R* ratio [11]. The model is given by

$$L = \frac{V_{base}^2}{P_{sc}} \frac{1}{2\pi f} \qquad (Eq.AII.52)$$

Where, the system inductance is represented by a relation of system voltage and short circuit capability. Through the manipulating of Eq. AII.52, it can be seen as

$$R = \frac{2\pi f L}{(X/R)} \qquad (Eq.AII.53)$$

Consequently, the higher the *X/R* ratio is, the lower the value of internal system resistance R, leading to a more significant synchronous machine short-circuit contribution [11]. Normally, this relationship is in order of 10 to 20 [12].

Finally, the impedance seen from the infinite bus as subnet is [12]

$$Z_Q = \frac{1.1 * V_{base}^2}{\sqrt{3} * V_{base} * I_{sc}} = \frac{1.1 * V_{base}^2}{P_{sc}} \qquad (Eq.AII.54)$$

In the following table, we can find the usual values of short circuit currents and powers for different line voltage values.

TABLE AII II
USUAL SHORT CIRCUIT CURRENTS AND POWERS FOR DIFFERENT LINE VOLTAGE VALUES [12]

| $V_{base}$ | $I_{sc}$ | $P_{sc}$ |
|---|---|---|
| 10 kV | 29 kA | 0.5 GVA |
| 110 kV | 42 kA | 8 GVA |
| 220 kV | 63 kA | 24 GVA |
| 380 kV | 80 kA | 53 GVA |

The model included in the *SimPowerSystems* toolbox is similar to the model developed in this research, it is called "*Synchronous Machine*" and also splits its equations in electrical and mechanical. However, in the electrical part it includes the *abc* to *qd* transformation and its inverse. The Fig. AII.15, Fig. AII.16 and Fig. AII.17 display them.

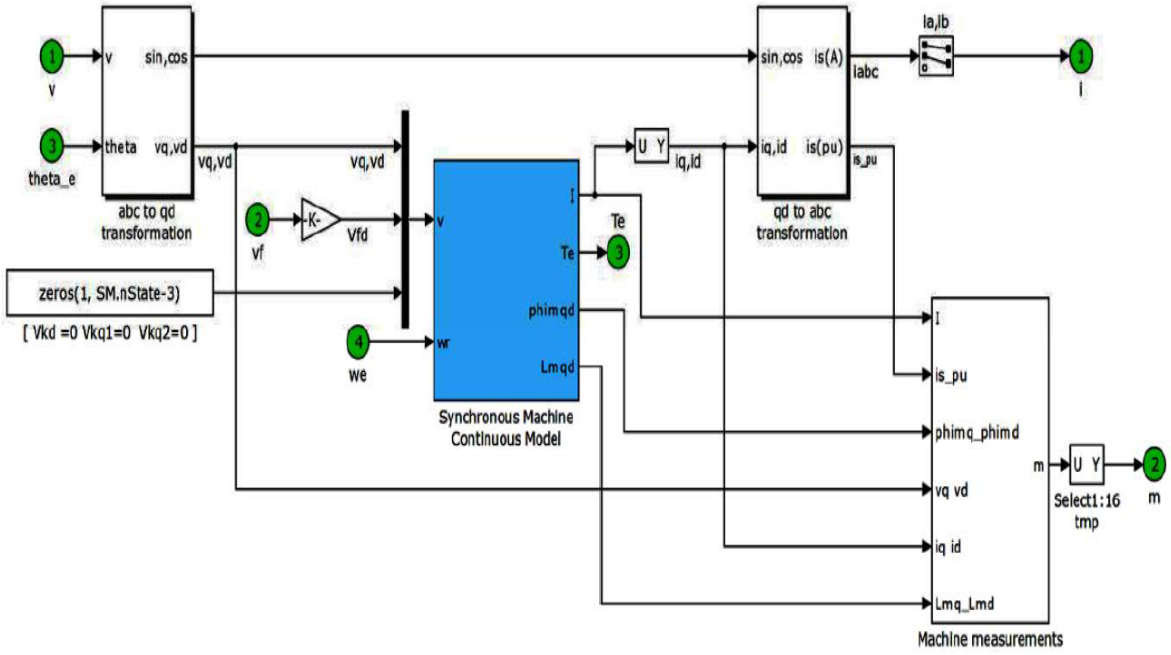


Fig.AII. 15. Block diagram of electrical model of synchronous machine in SimPowerSystems toolbox

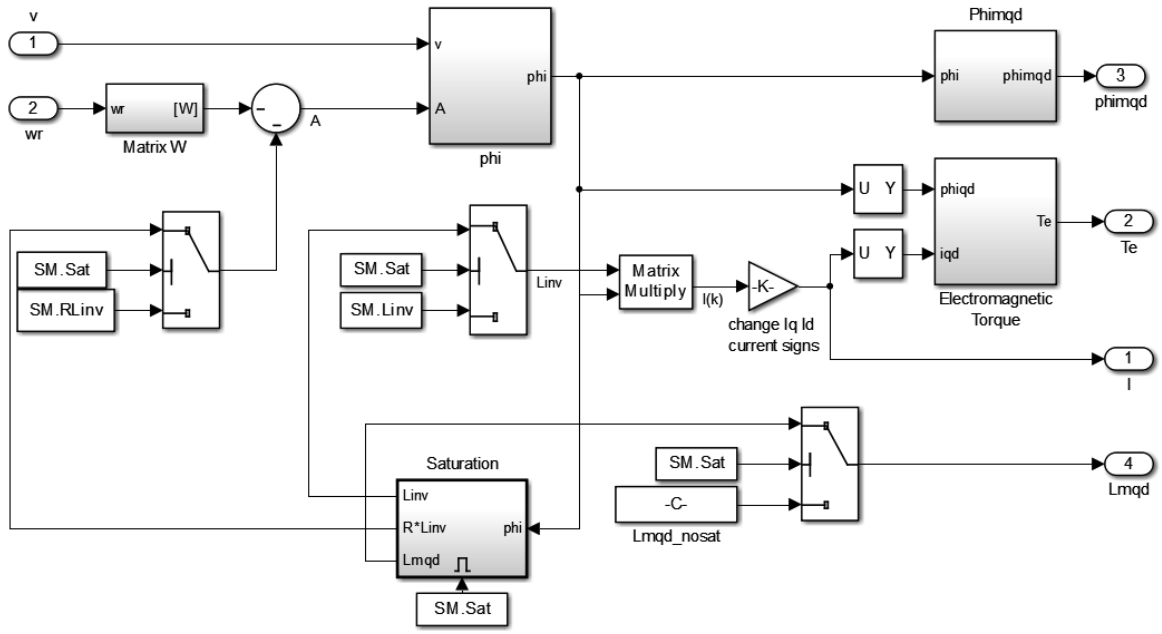


Fig.AII. 16. Internal block diagram of Synchronous Machine Continues Model in SimPowerSystems toolbox

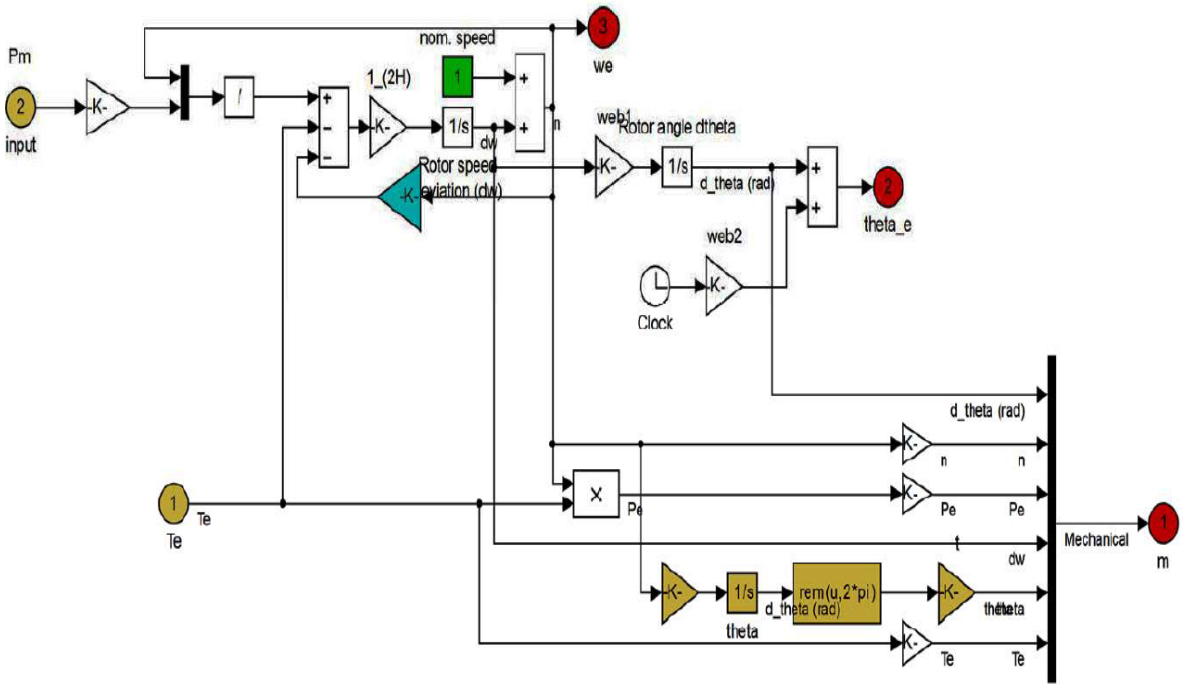


Fig.AII. 17. Block diagram of mechanical model of synchronous machine in SimPowerSystems toolbox

## ANNEX III: THEORY OF EXCITATION SYSTEMS AND *PSS*

### *III.I Excitation Systems*

The general functional block diagram is shown in Fig.AIII.1 and it indicates various synchronous machine excitation subsystems. These subsystems may include a $V_t$ transducer and load compensator, excitation control elements, an exciter and in many instances a *PSS* [13].

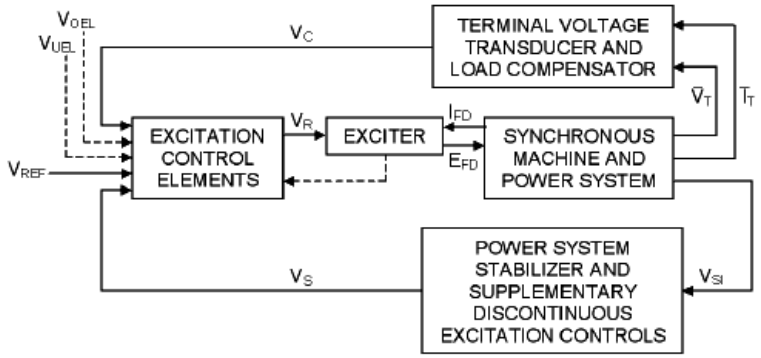


Fig.AIII. 1. General functional block diagram for synchronous machine excitation control system [13]

Three distinctive types of excitation systems are identified on the basis of excitation power source, as follows:

- *DC excitation systems,* which utilize a direct current generator with a commutator as the source of excitation system power.
- *AC excitation systems,* which use an alternator and either stationary or rotating rectifiers to produce the direct current needed for the synchronous machine field.
- *ST excitation systems*, in which excitation power is supplied through transformers or auxiliary generator windings and rectifiers.

In this research, we considered the DC type excitation system, exactly the model *DC1A*, because this model has been widely implemented by the industry and it is

the model ALSTOM uses for its computational studies. It is also used to represent other types of systems when detailed data and parameters for them are not available or when a simplified model is required.

We also implemented some key accessory functions common to most excitation systems as the voltage sensing, load compensation and the *PSS.*

A block diagram of the $V_t$ transducer and the load compensator is shown in Fig. AIII.2. The time constant, $T_R$, is used for the combined voltage sensing and compensation signal. Single-phase voltage and current sensing, in general, requires a longer time constant in the sensing circuitry to eliminate ripple.

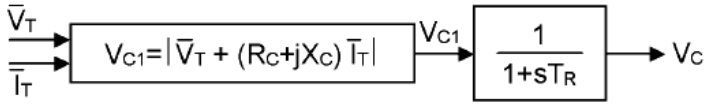


Fig.AIII. 2. Terminal voltage transducer and optional load compensation elements [13]

When load compensation is not employed ($R_C = X_C = 0$), the block diagram reduces to a simple sensing circuit. The $V_t$ of the synchronous machine is sensed and usually reduced to a dc quantity. While the filtering associated with the voltage transducer may be complex, it can usually be reduced, for modeling purposes, to the single time constant $T_R$. For many systems, this time constant is very small and provision should be made to set it to zero [13].

When compensation is desired, the appropriate values of $R_C$ and $X_C$ are entered. In most cases, the value of $R_C$ is negligible. Without load compensation, the excitation system, within its regulation characteristics, attempts to maintain a terminal voltage determined by the reference signal.

The Fig.AIII.3 shows the model *DC1A*. At the summing junction, $V_t$, the transducer output $V_C$, is subtracted from the set point reference, $V_{REF}$. The stabilizing feedback $V_F$, is subtracted and the *PSS* signal $V_S$, is added to produce an error voltage. In the steady state, the last two signals are zero, leaving only the $V_t$ error signal. The resulting signal is amplified in the regulator. The major time constant, $T_A$, and gain, $K_A$, are associated with the voltage regulator. These voltage regulators use power sources that are essentially unaffected by brief transients on the synchronous machine or auxiliary buses. The time constants, $T_B$ and $T_C$, may be used to model equivalent time constants inherent in the voltage regulator, but these time constants are frequently small enough to be neglected and provision should be made for zero input data [13].

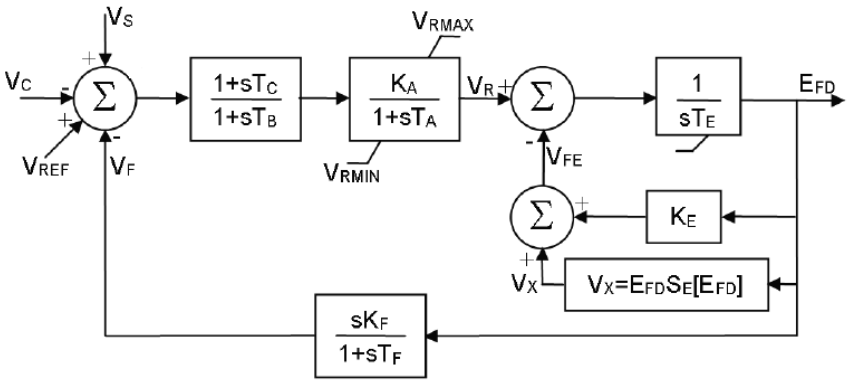


Fig.AIII. 3 Excitation System Type DC1A – DC Commuter exciter [13]

The voltage regulator output $V_R$, is used to control the exciter. When a self-excited shunt field is used, the value of $K_E$ reflects the setting of the shunt field rheostat. In some instances, the resulting value of $K_E$ can be negative and allowance should be made for this.

The term $S_E[E_{fd}]$ is a nonlinear function with values defined at two or more chosen values of $E_{fd}$. The output of this saturation block $V_X$, is the product of the input $E_{fd}$ and the value of the nonlinear function $S_E[E_{fd}]$ at this exciter voltage.

A signal derived from field voltage is normally used to provide excitation system stabilization, $V_F$, via the rate feedback with gain, $K_F$, and time constant, $T_F$ [13].

### *III.II Power System Stabilizers*

As we said before, in some cases the excitation system works together with one *PSS*, which has as basic function to add damping to the generator rotor oscillations, through excitation control on the excitation using an auxiliary stabilizing signal (*PSS* output). To provide and ensure a robust damping, the *PSS* must produce a component of electrical torque in phase with the rotor speed deviations, therefore, it should have and provide a moderate phase lead at the frequencies of interest in order to compensate for the inherent lag between the field excitation and the electrical torque induced by the *PSS* action.

Fig. AIII.4 shows the generalized form of a *PSS* with a single input. Some common stabilizer input signals, $V_{SI}$, can be either the machine speed deviation, $d\omega$, or its acceleration power, $P_a$.

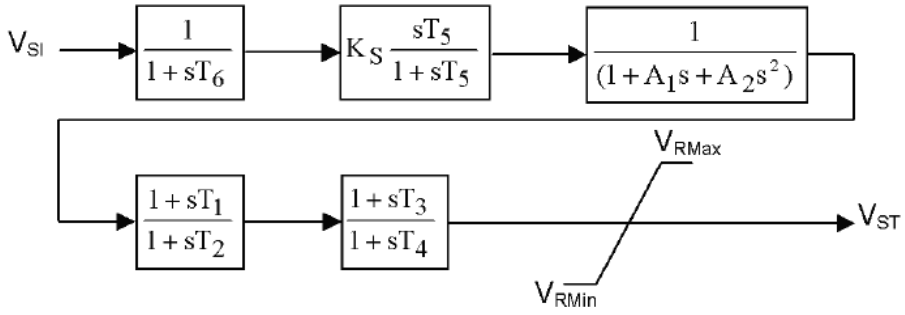


Fig.AIII. 4 PSS Type PSS1A – Single input [13]

The *PSS* representation in Fig. AIII.4 consists of a low-pass filter, a general gain, a washout high-pass filter, a phase-compensation system, and an output limiter.

$T_6$ may be used to represent a transducer time constant. The stabilizer gain $K_s$ determines the amount of damping introduced by the *PSS*. Ideally, the gain should be set at a value corresponding to maximum damping; however, it is often limited by other considerations. The *washout* high-pass filter, with the time constant $T_5$ high enough to allow signals associated with oscillations in $d\omega$ to pass unchanged. Without it, steady changes in speed would modify the terminal voltage. This filter allows the *PSS* to respond only to changes in speed. From the viewpoint of the *washout* function, the value of $T_5$ is not critical and may be in the range of 1 to 20 seconds. The main consideration is that it must be long enough to pass stabilizing signals at the frequencies of interest unchanged, but not so long that it leads to undesirable generator voltage excursions during system-islanding conditions [4].

In the next block, $A_1$ and $A_2$ allow some of the low-frequency effects of high-frequency torsional filters (used in some stabilizers) to be accounted for. When not used for this purpose, the block can be used to assist in shaping the gain and phase characteristics of the stabilizer, if required. The phase-compensation system is represented by a cascade of two first-order lead-lag transfer functions used to compensate the phase lag between the excitation voltage and the $T_e$ of the synchronous machine [4, 13].

Stabilizer output can be limited in various ways, not all of which are shown in Fig. AIII.4. This model shows only simple stabilizer output limits, $V_{STMAX}$ and $V_{STMIN}$.

The speed-based shaft stabilizers or $d\omega$ signal could be an input to the thermal units, but requires a careful consideration of the effects on torsional oscillations. The *PSS*, while damping the rotor oscillations, can cause instability of the torsional modes. One approach successfully used to circumvent the problem is to sense the speed at a shaft location near the nodes of the critical torsional modes. In addition to this, an electronic filter in the stabilizing path attenuates the torsional components. This is a disadvantage, because if it needs to use a torsional filter, it

also introduces a phase lag at lower frequencies [4]. The other option is when the input is a $P_a$ signal. The $P_a$ may be derived to a signal proportional to $d\omega$ and it does not contain torsional modes. At the end, the $P_a$ stabilizer has two major advantages over the $d\omega$ stabilizer. First, the $P_a$ signal has a high degree of torsional attenuation, and hence there is generally no need for a torsional filter in the main stabilizing path. This eliminates the stability problem of the exciter mode, thereby allowing a higher stabilizer gain, which results in better damping of system oscillations. The second advantage is that an end-of-shaft speed sensing arrangement, with a simple torsional filter, can be used with $P_e$ to derive the $P_m$ signal. This allows the use of a standard design for all units irrespective of their torsional characteristics [4]. For these reasons, the $P_a$ *PSS* has been chosen.

*SimPowerSystems* includes the scheme shown in Fig A.III.5 with its model called "*Excitation System*" for the excitation system type *DC1A* with terminal voltage transducer and load compensation elements.

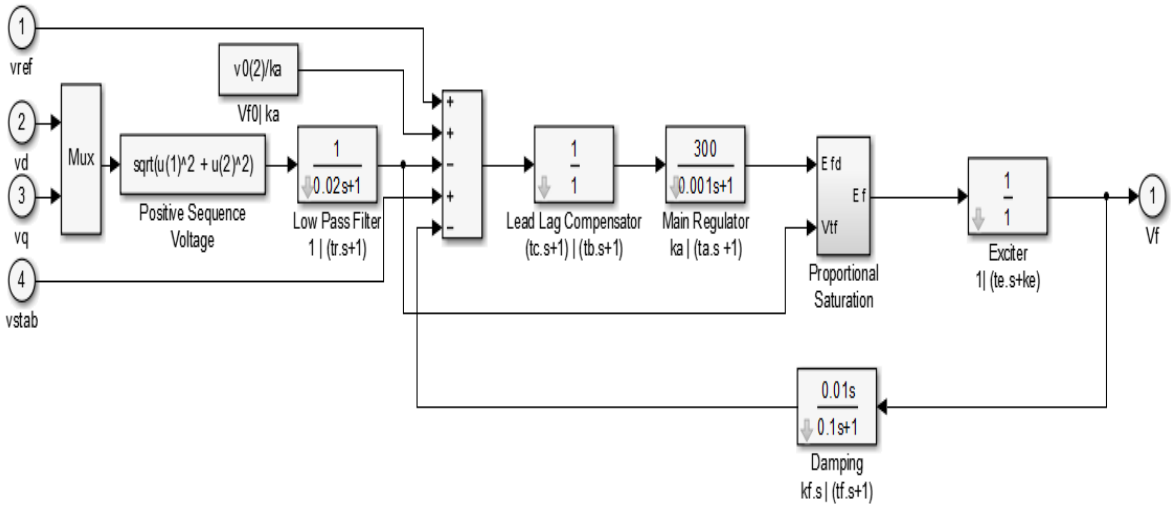


Fig.AIII. 5. The excitation model implemented by *SimPowerSystems*

Fig. AIII.6 shows the $P_a$_$PSS$ model implemented by *SimPowerSystems* with the model called "*Generic Power System Stabilizer*".

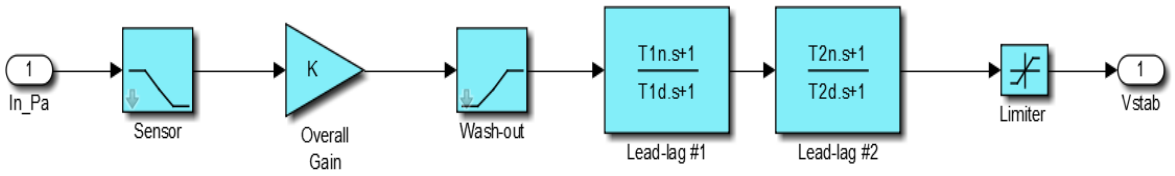


Fig.AIII. 6. The *PSS* model implemented by *SimPowerSystems*

### *III.III Tuning of Excitation System and PSS*

Knowing the type of excitation system and *PSS* to implement, the next step is to tune their parameters. Starting with the excitation system, the procedure is based on the emulation of the open-circuit step response. This is a standard control tuning practice used for several decades. When simulations with excitation system and *Gen* model data result in unacceptable responses, guidelines are provided for tuning models until well behaved, and thus, realistic, responses are achieved. Limits and other nonlinear parameters in exciter models are also very important when conducting simulations. They determine the exciter response following a large perturbation to the system [14].

As was mentioned early, the excitation system to implement is a *DC1A*, shown in Fig. A.III.3. We ignore Non-linearities, the constant times $T_C$ and $T_B$ are assumed equal to each other, thus cancelling, and the *Gen* is included. Figure A.III.6 shows *AVR* and exciter frequency response for a well-tuned excitation system. Tuning of this type of exciter must take care not only of the voltage-regulating loop stability, but also of the internal loop stability [14].

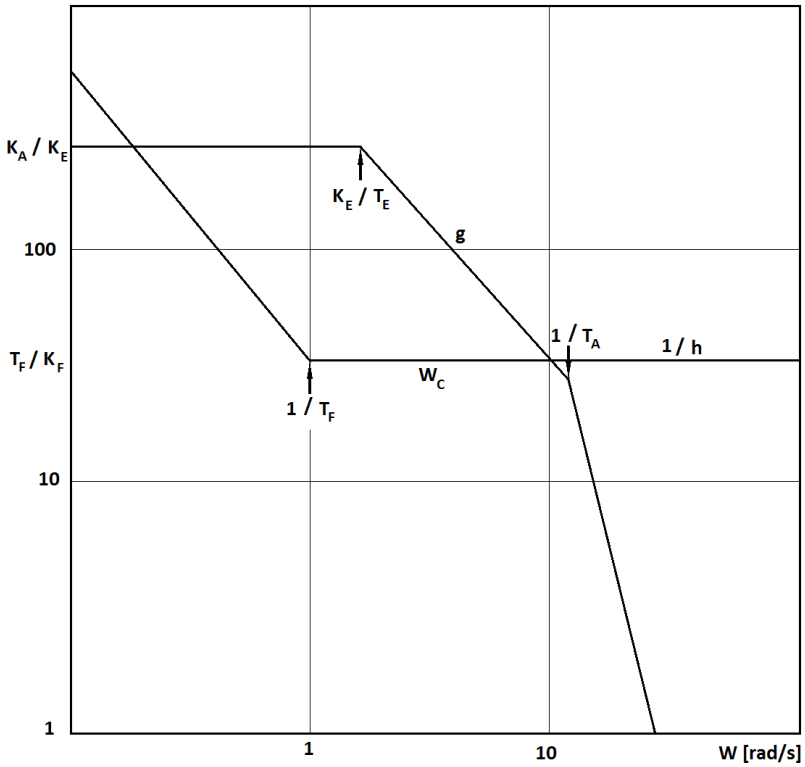


Fig.AIII. 7. Bode diagram of a well-tuned *DC1A* excitation system model.

The voltage-regulating loop remains stable as long as this loop's crossover occurs about halfway between $1/T_F$ and the second intersection frequencies. Halfway between those frequencies, the phase lag contributed by the *AVR*-Exciter system should be small, the main phase lag contribution at crossover being the -90 degrees due to generator field time constant. The internal loop is stable as long as its *gh* phase margin upon internal loop crossover is adequately high. Since internal loop crossovers occur when the magnitude of *gh* is equal to 1, the points of intersection between *g* and 1/*h* in Fig. AIII.7 are internal loop crossover points. The internal loop is then be adequately damped when the second intersection occurs at frequencies at or below $1/T_A$ [14].

With an open-circuit step response, the suggested tuning procedure has the following steps:

a. Compare $K_A$ $T_A$, $T_E$ and *T'do* with typical data. $K_A/K_E$ should be higher than 200, with $K_E$ close to zero or 1, $T_A$ and $T_E$ are dependent on *AVR* and exciter characteristics and *T'do* from the *Gen* features. Typical tuning parameters are $T_F$, and, particularly, $K_F$.

b. As an initial guess, we assume that the internal loop crossover occurs exactly at $1/T_A$. This means that:

$$K_A = \frac{T_F T_E}{T_A K_F} \qquad (Eq.\,AIII.1)$$

c. Under assumption b, we define an adequate size "*plateau*" for the external loop crossover:

$$T_F = 5T_A \qquad (Eq.\,AIII.2)$$

d. Within this plateau, crossover of the external loop must occur. The exact logarithmic halfway point between $1/T_A$ and $1/T_F$, is calculated using:

$$\log(W_C) = \log\left(\frac{1}{T_F}\right) + \frac{\log\left(\frac{1}{T_A}\right) - \log\left(\frac{1}{T_F}\right)}{2} \qquad (Eq.\,AIII.3)$$

then,

$$W_C = \frac{1}{T_A\sqrt{5}} \qquad (Eq.\,AIII.4)$$

External loop crossover occurs at this frequency as long as:

$$\log\left(\frac{T_F}{K_F}\right) - \log(1) = \log(W_C) - \log\left(\frac{1}{T'_{do}}\right) \qquad (Eq.\,AIII.5)$$

Replacing,

$$\frac{T_F}{K_F} = \frac{5T_A}{K_F} = \frac{T'_{do}}{T_A\sqrt{5}}\,, \qquad thus \quad K_F = \frac{T_A^2 5\sqrt{5}}{T'_{do}} \qquad (Eq.\,AIII.6)$$

e. The actual value of $K_A$ is now compared with the calculated in Eq.AIII.1

If $K_A$ is close to $(T_F T_E)/(K_F T_A)$, with $T_F$ and $K_F$ as calculated in Eq.AIII.2 and Eq.AIII.6, then use those $T_F$ and $K_F$ values as tuning parameters or any combination of $T_F$ and $K_F$ as long as the $T_F/K_F$ ratio is the same and as long as $T_F$ is greater than the value calculated Eq.AIII.2

If $K_A$ is much higher than $(T_F T_E)/(K_F T_A)$, we must try the values suggested above. If the step response is still too oscillatory, the only alternative is to check whether $K_A$ is adjustable, and if so, adjust it to $(T_F T_E)/(K_F T_A)$ and use the $T_F$ and $K_F$ values suggested above.

If $K_A$ is lower than $0.7(T_F T_E)/(K_F T_A)$, the second *g* and *1/h* intersection should occur at values lower than $1/T_A$. This second intersection can be chosen at a frequency:

$$W_{2nd} = \sqrt{\frac{2.236 K_A}{T'_{do} T_E}} \qquad (Eq.AIII.7)$$

And the new $T_F$ and $K_F$ values can be calculated by

$$T_F = \frac{5}{W_{2nd}} \qquad and \qquad K_F = \frac{11.18}{T'_{do} W_{2nd}^2} \qquad (Eq.AIII.8)$$

Taking the following sample data recommended by IEEE [13],

$$K_A = 46 \qquad T_A = 0.06 \qquad T_E = 0.46 \qquad K_E = 1 \qquad T'_{do} = 6.22$$

Thus, the values tuned from Eq. AIII.2, Eq.AIII.8 and Eq.AIII.1 are:

$$T_F = 0.3 \qquad K_F = 0.0065 \qquad K_A = 355.4462$$

Since the $K_A$ tuned value is higher than its assumed value, we take $K_A$ as a tunable parameter, and its new value is the tuned value.

Having the new gain and assumed to be nonadjustable, then $T_F$ can be tunable at 0.5*s*, so $K_F$, is chosen at

$$K_{Fnew} = \frac{K_{Fold} T_{Fnew}}{T_{Fold}} \qquad (Eq.AIII.9)$$

We repeat the steps above until the conditions mentioned in paragraph *e* are fulfilled.

The results are compared with the MatLab default values in the Fig. AIII.8 and Fig. AIII.9.

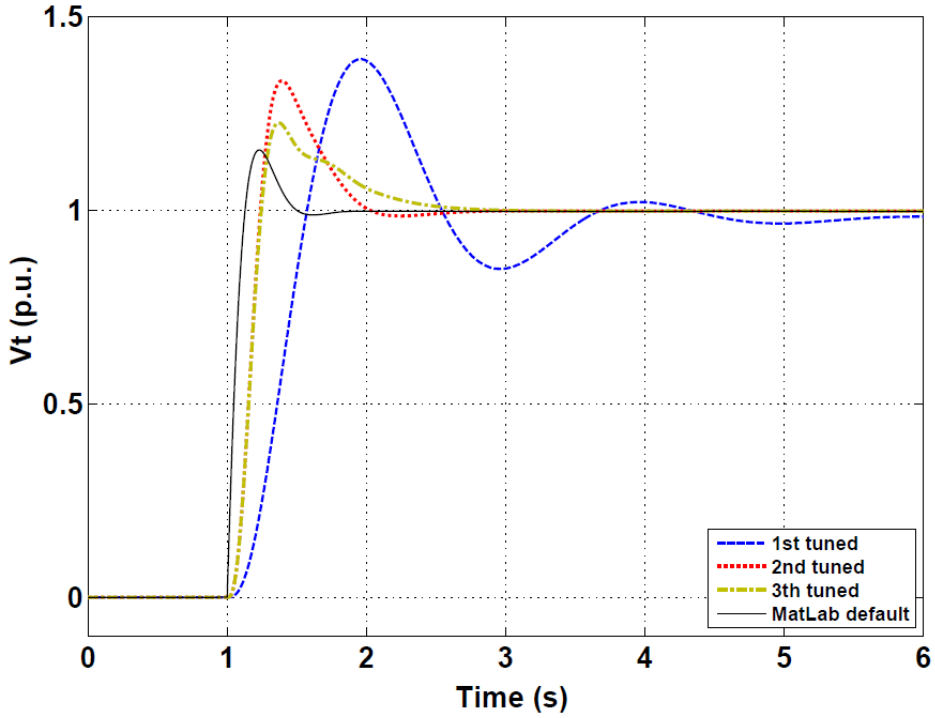


Fig.AIII. 8. Terminal Voltage open-circuit step response of *DC1A* model.

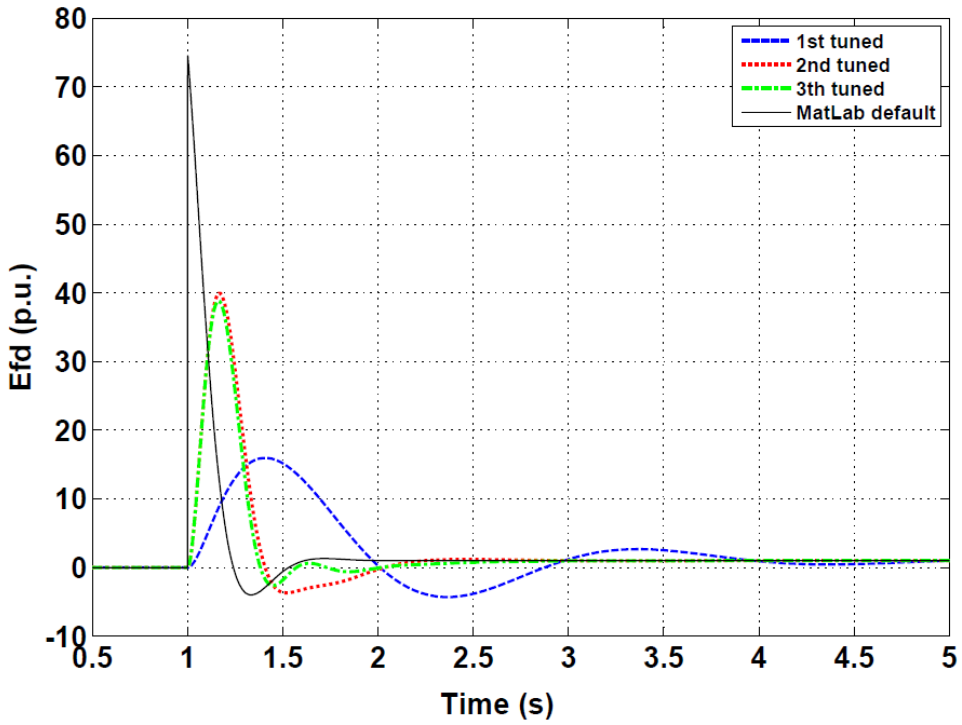


Fig.AIII. 9. Field Voltage open-circuit step response of *DC1A* model.

The default parameters values of the *PSS* in MatLab are:

$$T_{sensor} = 30ms \quad Gain = 20 \quad T_{wo} = 2s \quad T1_n = 50ms \quad T1_d = 20ms$$
$$T2_n = 3s \quad T2_d = 5.4s$$

After making a considerable number of simulations, the following parameters were found to be acceptable to make the research possible:

$$T_{sensor} = 5ms \quad Gain = 3.1250 \quad T_{wo} = 1s \quad T1_n = 60ms \quad T1_d = 1s$$
$$T2_n = 0s \quad T2_d = 0s$$

The responses of its performance are shown in Fig. AIII.10 without a disturbance applied and in Fig. AIII.11 with a disturbance applied.

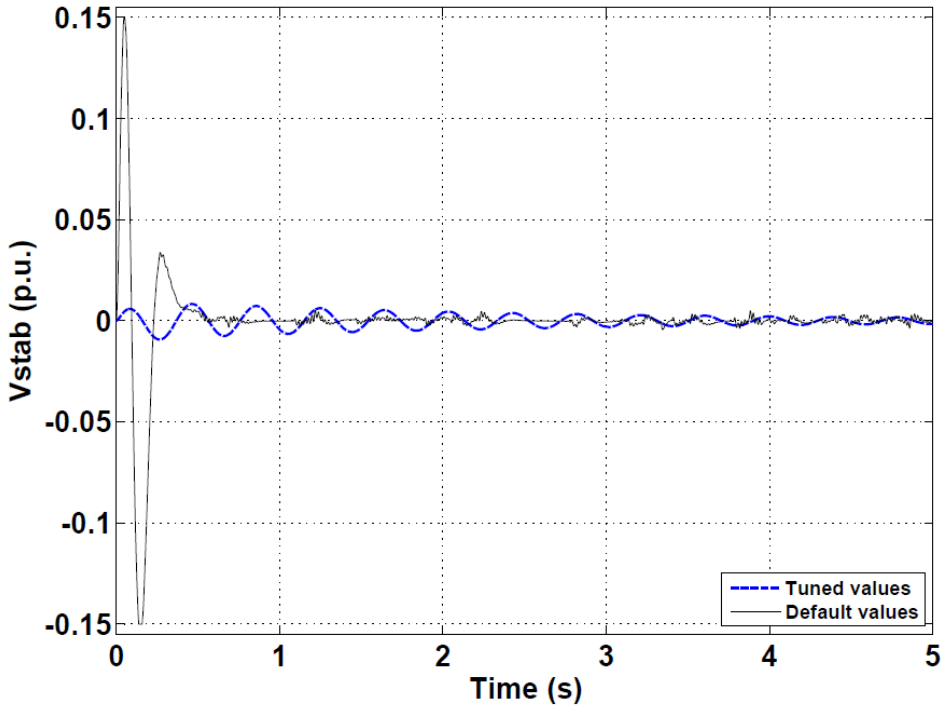


Fig.AIII. 10. Responses of *PSS* with tuned and default values without disturbance applied.

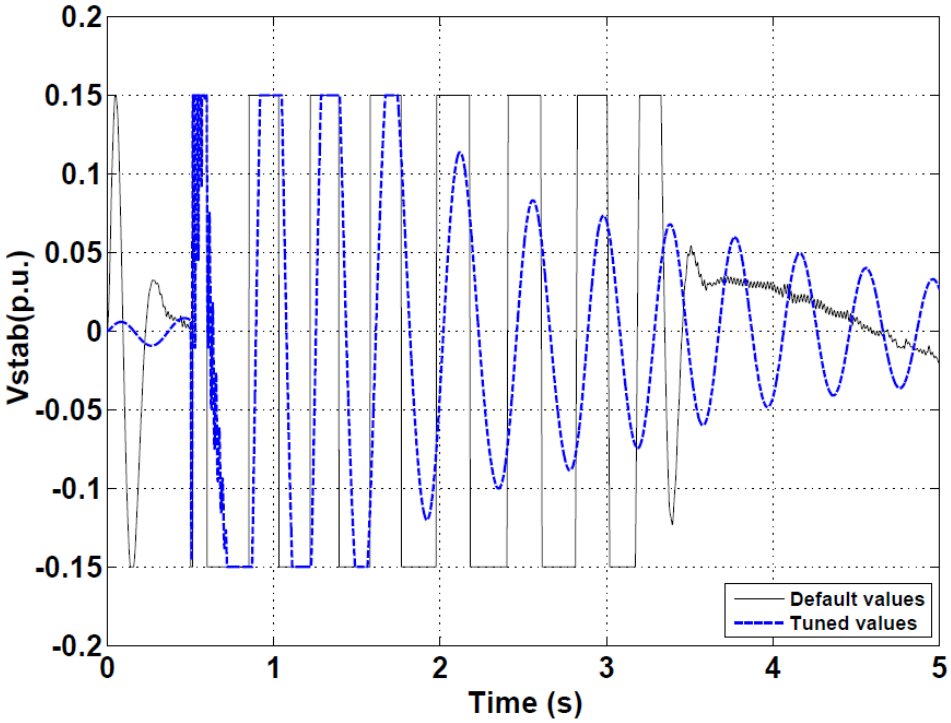


Fig.AIII. 11. Responses of *PSS* with tuned and default values with disturbance applied at $t$=80ms.

## ANNEX IV: TUNING OF THE *ST* SPEED GOVERNOR

By default in *SimPowerSystems*, the speed controller is modeled in the speed governor system of the turbine as a proportional regulator or permanent droop speed, which is $1/R_p$ as was shown in the Fig AI.6. Then, the controller is *P* type and his value by default is 20 ($R_p = 0.05$).

The Fig.AIV.1 shows a structure to tune a *PID* controller for a plant. With the mathematical model of the plant, it is possible to apply different techniques in order to determine a set of controller parameters that fulfills the specifications of the closed loop system. In other words, the system can be tuned.

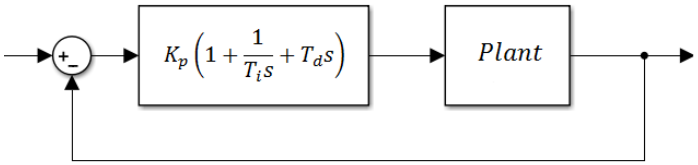


Fig.AIV. 1. Scheme for tune a controller of one plant

In this research, we tuned the controller using the method proposed by Ziegler and Nichols, which involves applying an open-loop step input to the system. If the mathematical model of the plant does not contain integrators or complex conjugate dominant poles, the response curve to a step input may be S-shaped, as shown in Fig.AIV.2. Such step-response curves can be generated experimentally or, as in this case, from a dynamic simulation.

The controller is described by the follow transfer function:

$$K_p\left(1+\frac{1}{T_i s}+T_d s\right) \qquad (Eq.AIV.1)$$

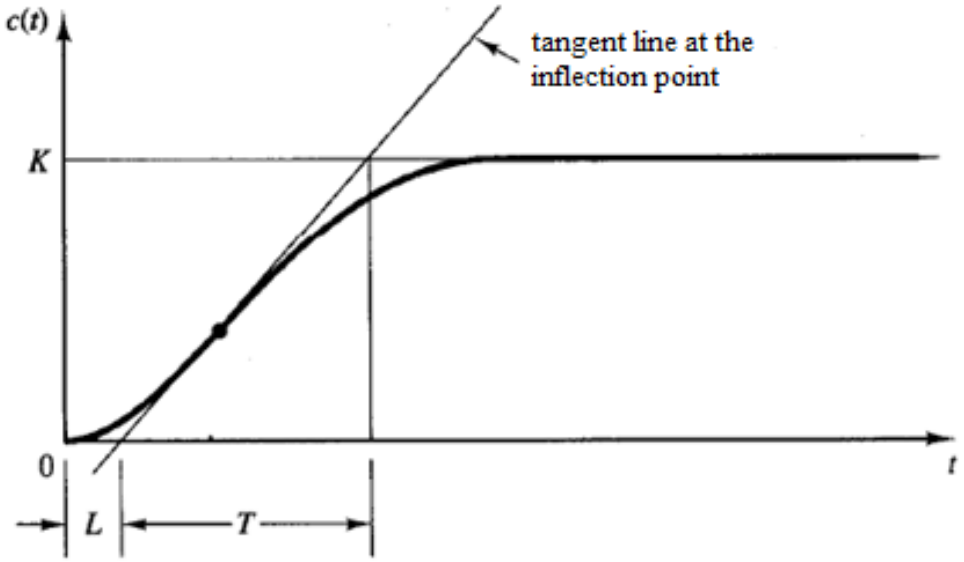


Fig.AIV. 2. Response curve in S-shape for tune a controller [15]

As seen in Fig.AIV.2, the S-shape curve is characterized by two parameters: the delay time *L* and the time constant *T*. These parameters are determined by drawing a tangent line at the inflection point of the S-shape curve. The intersection of the tangent line with the time axis is the *L* value. The projection on the *x-axis* of the intersection of the tangent line with the line $y(t) = K$, minus *L* is the value of *T*, as shown in Fig. AIV.2.

Once *L* and *T* are obtained, we calculate the constants ($K_p$, $T_i$, $T_d$) of the controller using the table AIV.I.

TABLE AIV. I
ZIEGLER- NICHOLS TUNING RULES BASED ON SLOPE INPUT TO A PLANT [15]

| Controller Type | $K_p$ | $T_i$ | $T_d$ |
|---|---|---|---|
| *P* | T/L | ∞ | 0 |
| *PI* | 0.9T/L | 10L/3 | 0 |
| *PID* | 1.2T/L | 2L | 0.5L |

In this case, the dynamic model of the plant is formed by 3 stages: The servomotor of the valves, the turbine and the generator. The behavior of the stages can be described by simplified transfer functions.

The transfer function to describe the speed relay and the servomotor is

$$\frac{1}{1+T_{SM}s} \qquad (Eq.AIV.2)$$

A simplified transfer function of the turbine relating perturbed values of the turbine torque ($\Delta T_m$) and *CV* position ($\Delta V_{CV}$) maybe written as follows

$$\frac{\Delta T_m}{\Delta V_{CV}} = \frac{F_{HP}}{1+sT_{CH}} + \frac{1-F_{HP}}{(1+sT_{CH})(1+sT_{RH})} = \frac{1+sF_{HP}T_{RH}}{(1+sT_{CH})(1+sT_{RH})} \qquad (Eq.AIV.3)$$

In the above transfer function, it is assumed that $T_{CO}$ is negligible in comparison with $T_{RH}$.

The *Gen*, is represented by the simpler transfer function based on $T_M$ and $K_D$ constants, combining Eq. AII.29 and Eq. AII.30 by

$$\frac{1}{T_M s + K_D} \qquad (Eq.AIV.4)$$

From Fig. AIV.1, the scheme is

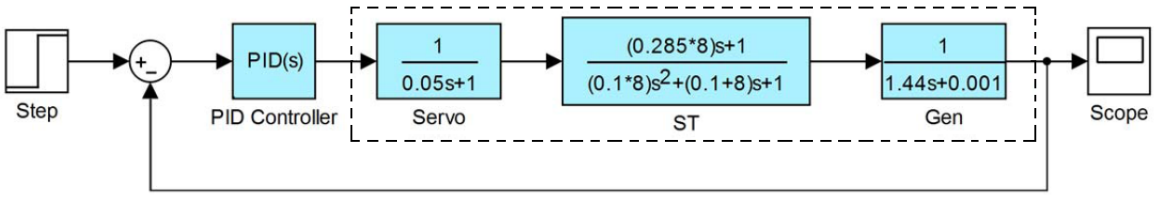


Fig.AIV. 3. Diagram block to tune the controller for a plant

Employing the method proposed by Ziegler and Nichols, the scheme changes to

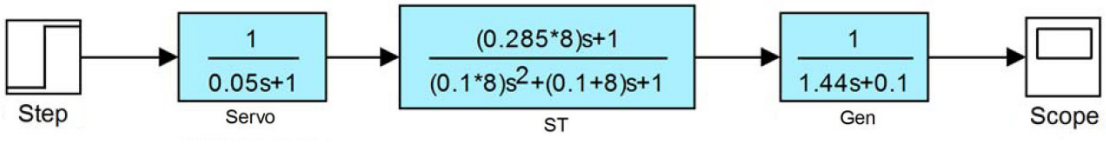


Fig.AIV. 4. Diagram for tune the controller with Ziegler-Nichols method

The output obtained from the system is shown in the Fig. AIV.4 is

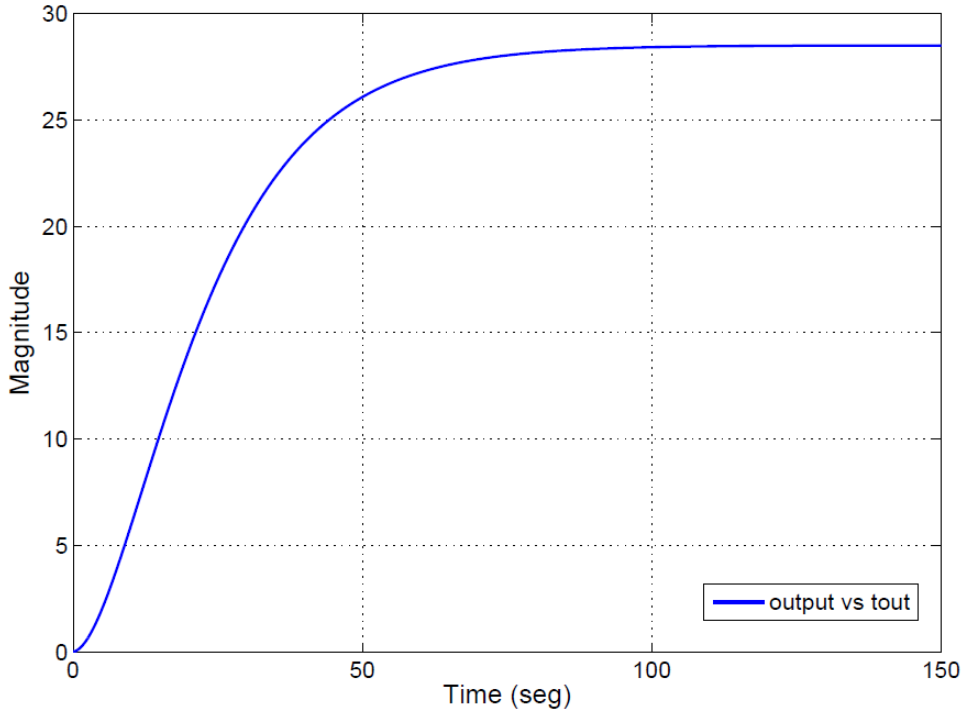


Fig.AIV. 5. Output of step input with open loop

To obtain the equation of the curve shown in Fig. AIV.5, we used MatLab's *Curve Fitting Toolbox*, which is a collection of graphical user interfaces (GUIs) and M-file functions for curve and surface fitting that operate in the MatLab technical computing environment. It has as main features data fitting using parametric and non-parametric models. The toolbox includes a library of parametric models, with polynomials, exponentials, rational, sums of Gaussians, Fourier polynomials, and

many others. To open *Curve Fitting Tool*, type on the command window the follow instruction *cftool*.

The kind of fit chosen was 9th degree polynomial, the results are:

Iteration limit reached for robust fitting.

Linear model Poly9:
f(x) = p1*x^9 + p2*x^8 + p3*x^7 + p4*x^6 +
p5*x^5 + p6*x^4 + p7*x^3 + p8*x^2 + p9*x + p10
Coefficients (with 99% confidence bounds):}
p1 = -2.537e-016 (-2.575e-016, -2.499e-016)
p2 = 1.93e-013 (1.904e-013, 1.956e-013)
p3 = -6.297e-011 (-6.37e-011, -6.224e-011)
p4 = 1.151e-008 (1.139e-008, 1.162e-008)
p5 = -1.288e-006 (-1.298e-006, -1.278e-006)
p6 = 9.011e-005 (8.955e-005, 9.068e-005)
p7 = -0.003779 (-0.003797, -0.003761)
p8 = 0.07753 (0.07721, 0.07784)
p9 = 0.1249 (0.1225, 0.1274)
p10 = -0.0939 (-0.1001, -0.08771)

Goodness of fit:
SSE: 1.663
R-square: 1
Adjusted R-square: 1
RMSE: 0.01883

The equation that describes the curve with its coefficients based on the method is

$$-2.537e^{-16}x^9 + 1.93e^{-13}x^8 - 6.297e^{-11}x^7 + 1.151e^{-8}x^6 - 1.288e^{-6}x^5 + 9.011e^{-5}x^4 - 3.779e^{-3}x^3 \quad - 7.753e^{-2}x^2 + 0.1249x - 0.0939 \qquad (Eq.AIV.5)$$

The curve fitted described by Eq. AIV.5 and the open loop step response are shown in Fig. AIV.6

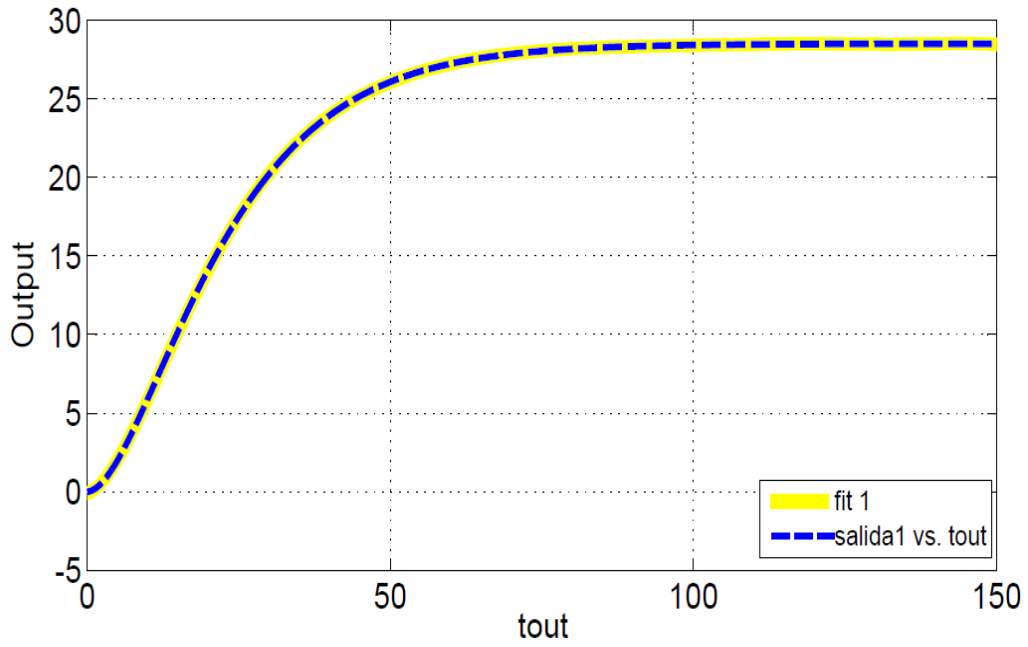


Fig.AIV. 6. Analysis of curve fitted described by Eq. AIV.5

The following code was used to find the inflection point and to draw the tangent line to the curve, needed to obtain the values of *L* and *T*:

```
>> p1 = -2.537e-016;
>> p2 =  1.93e-013;
>> p3 = -6.297e-011;
>> p4 =  1.151e-008;
>> p5 = -1.288e-006;
>> p6 =  9.011e-005;
>> p7 =  -0.003779;
>> p8 =    0.07753;
>> p9 =     0.1249;
>> p10 =    -0.0939;
>> syms x;
>> y=p1*x^9 + p2*x^8 + p3*x^7 + p4*x^6 + p5*x^5 + p6*x^4 + p7*x^3 + p8*x^2 + p9*x + p10;
>> dy=diff(y);
>> d2y=diff(dy);
>> inflec_pt=solve(d2y);
>>double(inflec_pt)
ans =
  1.0e+002 *
   1.5501
   0.8059
   0.1212
   1.1535 - 0.2881i
   0.5663 - 0.2753i
```

```
  0.5663 + 0.2753i
  1.1535 + 0.2881i
>> inflec_pt=inflec_pt(3);
>> double(inflec_pt)
ans =
  12.1239
>> subs(x,inflec_pt)
ans =
   17.3674
```

As we can observe, the inflection point is 12.1239 because the others were complex numbers or were out of range as 80.59 or 155.01. The image of the inflection point is 17.3674.

With the inflection point of the curve, the tangent line is found, taking two points around it. The points taken were (17.4, 12.1424) and (17.3, 12.0625) and thus the equation of the line is

$$y = 0.7990x - 1.7602 \qquad (Eq.AIV.6)$$

To find the value of *L*, we find the *x* intercept of the tangent line, making *y=0*. The value obtained is *L*= 2.2030. For *T*, we replace *y*=28,52 in the tangent line equation, and subtract the value of *L* from the x coordinate found. Then the value of *T* is 35.6970.

In the Fig. AIV.7, we can observe how the above values of *L* and *T* were found.

Replacing those values in the table AIV.I, the parameters obtained for the three kind of controllers, using the method proposed by Ziegler and Nichols, are shown in the table AIV.II

The performance of the tuned controllers and the default *P* controller from *SimPowerSystems*, are compared in Fig. AIV.8, which shows the step response of the system.

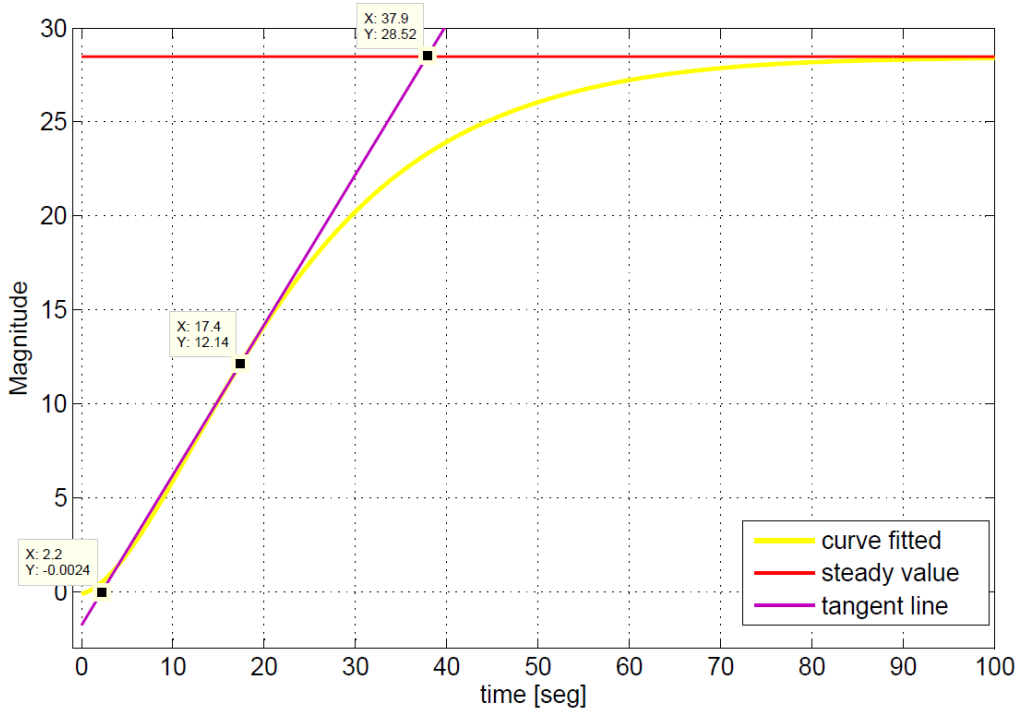


Fig.AIV. 7. Response curve of the speed governor, tangent line at infection point and steady value to find L and T values

With the results obtained from Fig. AIV.8, we see that the controller with the best performance is the *PID*.

TABLE AIV. II
VALUES OF PARAMETERS FOR THE DIFFERENTS TYPES OF CONTROLLERS PROPOSED BY ZIEGLER AND NICHOLS

| Controller Type | $K_p$ | $T_i$ | $T_d$ | *P* | *I* | *D* |
|---|---|---|---|---|---|---|
| *P* | 16.2038 | ∞ | 0 | 16.2038 | 0 | 0 |
| *PI* | 14.5834 | 7.3433 | 0 | 14.5834 | 1.9859 | 0 |
| *PID* | 19.4446 | 4.4060 | 1.1015 | 19.4446 | 4.4132 | 21.4182 |

From this starting point, the MatLab/Simulink *PID tuner* toolbox can perform a fine tuning of the controller. It is based on the next equation

$$P + I\frac{1}{s} + D\left(\frac{Ns}{s+N}\right) \qquad (Eq.AIV.7)$$

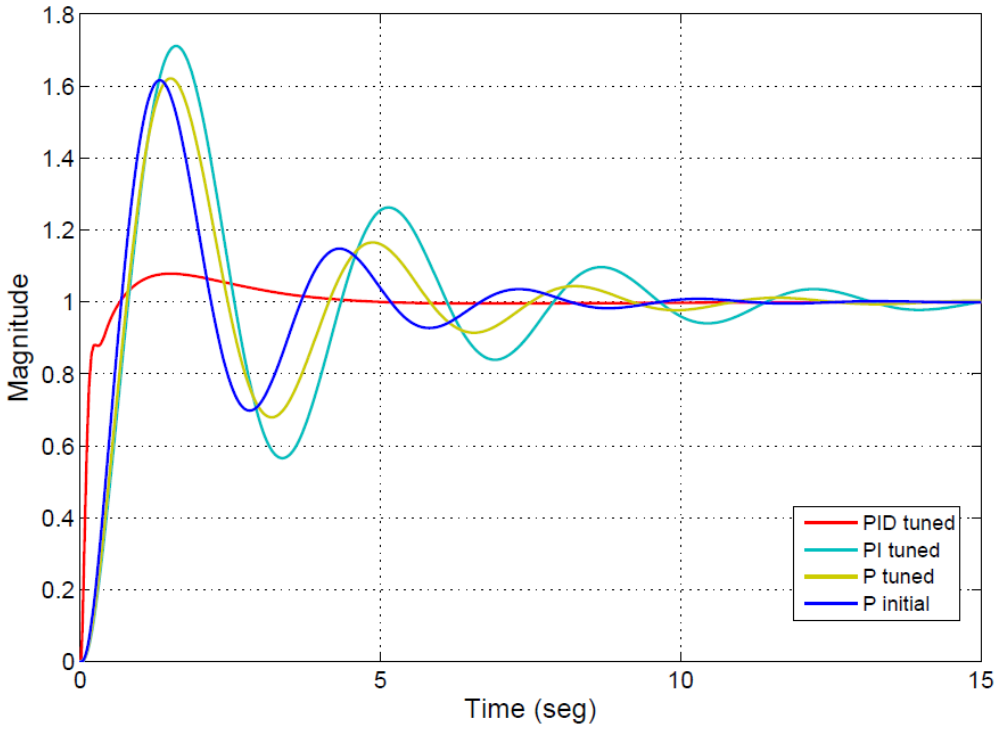


Fig.AIV. 8. Responses of the types of controllers proposed by Ziegler and Nichols and the SimPowerSystems by default

The derivative term is implemented using a more realistic $s/(s/N+1)$ transfer function, which gives more robustness to the Eq. AIV.1. The transfer function is a first-order pole filter and the filter coefficient *N* sets the location of the pole in the derivative filter.

The results obtained using the *PID tuner* toolbox are shown in the Fig. AIV.9. Also, table AIV.III summarizes the most important features of each controller.

The proportional, integral, and derivative gain parameters gave from the *PID tuner* toolbox are:

$$P = 87.6487 \qquad I = 11.2402 \qquad D = 31.7955 \qquad N = 160.8224 \qquad (Eq.AIV.8)$$

TABLE AIV. III
PERFORMANCE AND ROBUSTNESS OF EVERY TYPE OF CONTROLLER STUDIED

| Features / Controller Type | *P default* | *P tuned* | *PI tuned* | *PID tuned* | *PID tuned by toolbox* |
|---|---|---|---|---|---|
| *Rise time (sec)* | 0.45 | 0.513 | 0.53 | 0.352 | 0.0846 |
| *Settling time (sec)* | 7.8 | 10.2 | 14.2 | 3.25 | 1.56 |
| *Overshoot (%)* | 61.6 | 62.1 | 71.1 | 7.85 | 8.32 |
| *Peak* | 1.62 | 1.62 | 1.71 | 1.08 | 1.08 |

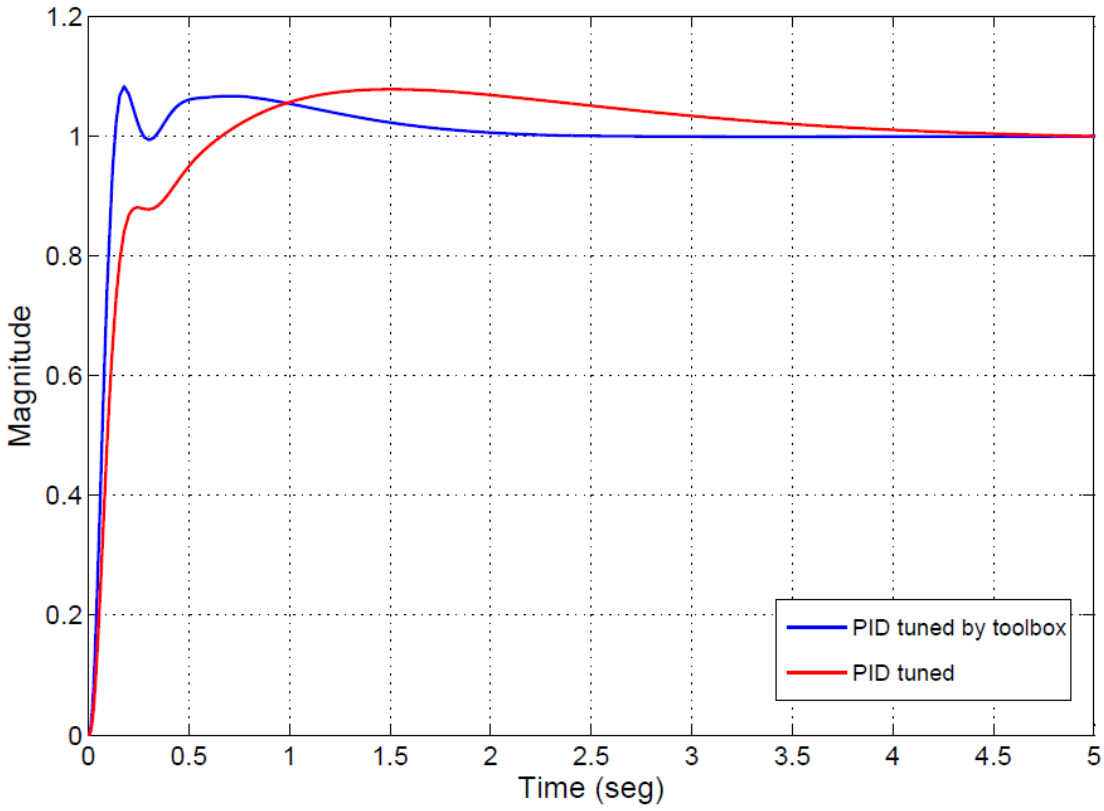


Fig.AIV. 9. Responses of PID proposed by Ziegler and Nichols and the PID tuned by *PID tuner* toolbox

As can be noted, the *P* and *PI* controllers proposed by the Ziegler and Nichols method do not outperform the default *P* controller. However, both *PID* controllers have better performances, which are shown in the table AIV.IV.

Based on these results, the controller considered in this research is the PID with the values tuned by the toolbox *PID tuner*.

TABLE AIV. IV
PORCENTAGE OF IMPROVEMENT ON THE PERFORMANCE OF THE PID CONTROLLERS

| **Features / Improvement** | ***PID tuned*** | ***PID tuned by toolbox*** |
|---|---|---|
| *Rise time (sec)* | 21.7778 % | 81.2 % |
| *Settling time (sec)* | 58.3333 % | 80 % |
| *Overshoot (%)* | 87.2565 % | 86.4935 % |
| *Peak* | 33.3333 % | 33.3333 % |

## ANNEX V: *FAST VALVING* CONTROL

As was mentioned early in the paper, the community considers *FV* an effective, inexpensive and adaptable control technique to improve and support the stability margins of the power system, applied to steam *PP*.

*FV* application consists of a fast control to decrease the $P_m$ input to the *ST*. This can be accomplished through a fast close or opening of *CV* and *IV*. On some units, high-pressure and reheat stop valves may also be tripped.

*FV* control is designed for non-continuous usage; its actuation is independent of the rest of the control systems of the *ST*. That is also possible, because to achieve the extremely rapid control necessary to limit *ST* overspeed, following a full rejection, the normal speed control and valve stroking rates are not fast enough. Besides this, the normal speed governor action also limits rotor acceleration, but has little effect in the critical time interval for first swing stability [16].

For those reasons, *FV* launching needs an independent control system to develop its performance. We already have seen how the actuation of the technique works, based on the strategy of *RACKE* and rotor angular $d\omega$ plus the action of the *PLU*. This annex focuses on the mathematical description of the valve stroke characteristic when *FV* is acting. The mathematical model is shown in Fig. 4 of the paper. Similarly, the stroke characteristic curve of the valve is shown in Fig. 1 while *FV* is applied.

After the launching of *FV*, the trigger signal switches the control, from the prime governor to the FV control block and activates it.

To describe the block diagram, we split it in two parts, calling them: the upper and the lower part. The first element is a delay with value of T1*s*, which simulates the

time delay between the launching of the trigger signal and the time when the valve begins to close, as is shown in Fig. AV.1(a). In the upper part, the trigger signal already with delay T1*s*, passes through an integrator. Its output is a line with a slope of *1/T2*, which means T2*s* is the time to reach the position 1 starting from 0. Figure AV.1(b) shows this.

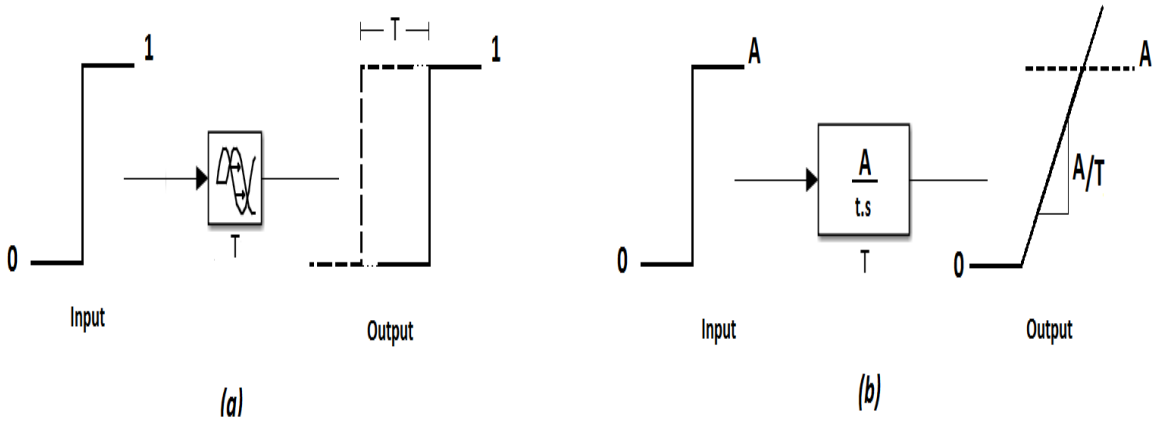


Fig.AV. 1. *(a)* Responses of *delay block (b)* Responses of *integrator block*

The signal is reflected on the x-axis (flip vertical) due to the operation of inverse or subtraction. Then, it is added to the output from the integrator, but delayed by T2*s*, ensuring that the time to decrease one unit (1p.u.) of the stroke is T2*s*. Here T2 is the valve closing time. This operation is shown in Fig. AV.2. The upper part simulates the actuation delay and the valve closing time.

The lower part has operators similar to those of the upper part. The trigger signal with delay T1*s*, passes through the integrator with *SFV*/T4 slope. After this, the signal takes a delay time of (T2 + T3), where T3 is the time during which the valve remains closed, also known as dead time. The signal is delayed again, this time by T4*s*, where T4 is the valve reopening time. The resulting signal is reflected on the x-axis (flip vertical) due to the operation of inverse or subtraction and it is added to the output of the integrator after a time delay of (T1+T2+T3) plus “pi” (the value

p.u. of steam flow through the *IV*). In this research, the *Gen* was implemented at nominal rate and operating in steady state at t=0. With this considerations, the value of the steam flow through *IV* when *FV* is released is the unit. The lower part simulates the dead time and the valve opening time until the position *SFV*. These operations are shown in Fig. AV.3.

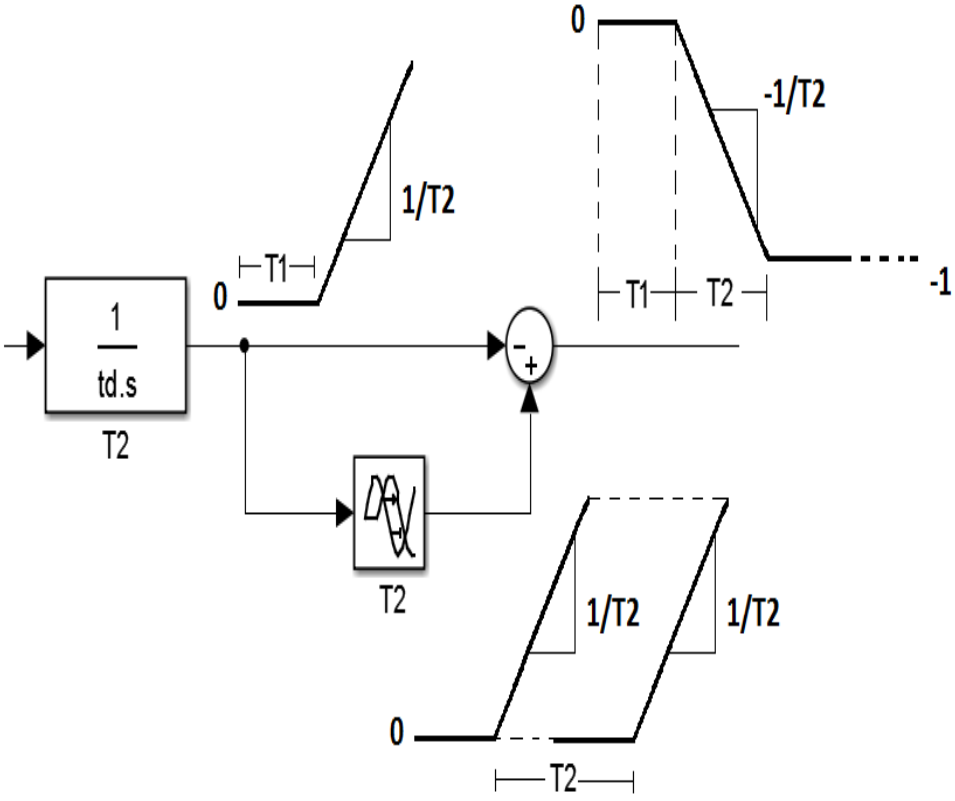


Fig.AV. 2. Responses of the first blocks and operator in the upper part of the *FV* mathematical model

The last part is the addition of the upper part plus the lower part. This generates the valve stroke characteristic curve in a conventional *FV* acting. To ensure that the position or stroke is in the acceptable range (0 p.u. to 1 p.u.), a limiter is added at the end of the model.

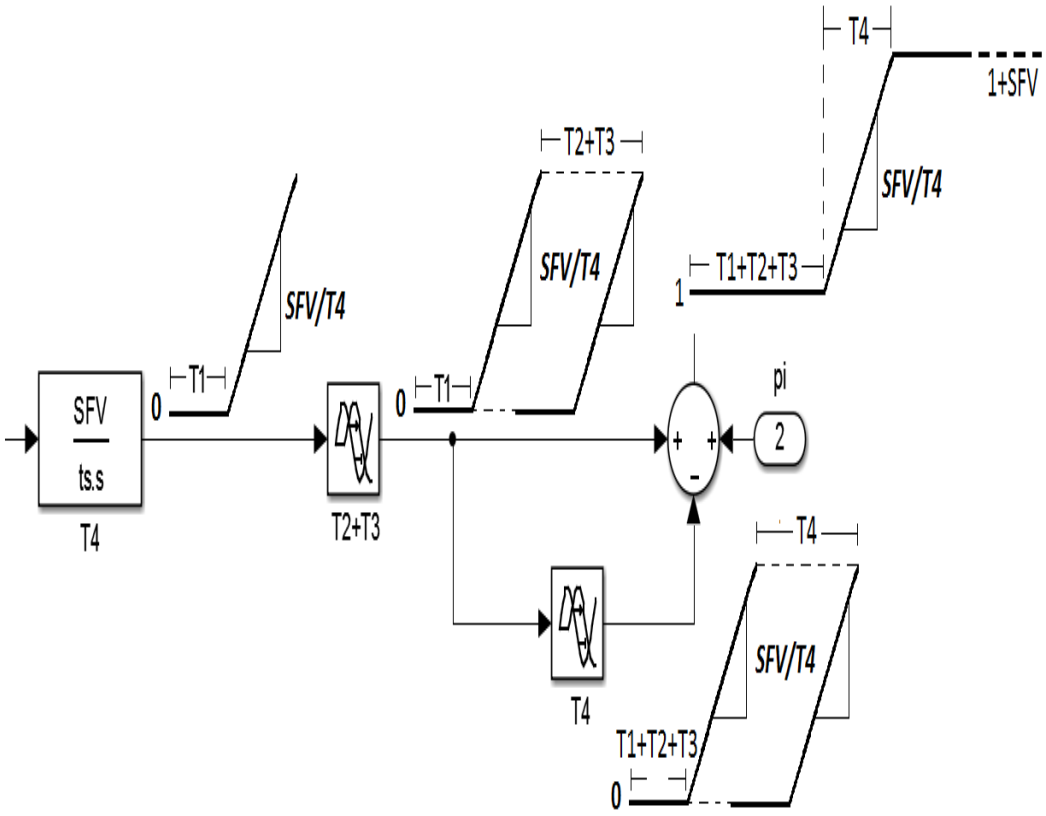


Fig.AV. 3. Responses of the blocks and operators in the lower part of the *FV* mathematical model

## ANNEX VI: EFFECTS OF *FV* ON THE *ST* AND ITS CONTROL SYSTEM

The consensus is that the *ST* and controls, rides through the load changes with very little disturbance provided that valves are fully open within approximately 11 seconds from initiation of *FV* [16]. When *FV* is released to support the transient stability and frequency grid, the action of faster opening/closing leads to a typical temperature variation of the steam from the heat recovery steam generator (*HRSG*). The resulting thermal stresses are no problem for the critical parts of the *HP* and *IP* valves. However, if the temperature variation of the life steam gets higher than an expected quantity, the low cycle fatigue (*LCF*) behavior of the *HP* valves can be affected. When *FV* is actuating with increasing power, it also exposes the *HP* and *IP* rotors to *LCF*, but the thermal stresses are, again, not a problem for the critical parts of the rotor, as long as their material fulfills several features. For example, for some materials *LCF* limits the number of cycles drastically [17].

The throttling of the *CV* leads to higher pressures in the *HRSG*. The relationship stroke versus mass flow and pressures of the valves are nonlinear, and then higher pressures appear when the valve reaches lower stroke values. These higher pressures are applied to the *HP* and *IP* blading as soon as the valves act.

For these reasons, the required throttling is made and defined by heat balances. These balances show calculations of the *HRSG* and the *ST* cycle. Some of the heat balances show, besides the thermodynamic state in front of the *HP* and *IP* valves, the pressure behind the valves, which is the pressure between the valves and blades.

About the control system, conventional *ST* controls and controlled elements would not have time to react appreciably to such a rapid momentary reheat flow

interruption. However, in the initial design stages, the entire plant control and protection scheme must be studied and perhaps some minor modifications made to assure compatibility with *FV* control. For instance, the coordinated or integrated type control systems, which utilize megawatt error, must have additional logic incorporated in order to respond properly. Also, when a turbine stage pressure is utilized for control purposes, the fluctuations accompanying *FV* must be taken into account [16].

### *VI.I Mechanical integrity of the valves*

For the operation mode where *FV* is applied, the *CV* and *IV* throttle the steam continuously. A supporting action consists of momentary fast opening or fast further closing, returning to their initial stroke position later. The main mechanical burden of the valves is the continuous throttling.

To avoid this, the main stop valve (*MSV*) and the intercept stop valve (*ISV*), in front of the *CV* and *IV* respectively, are included since some years ago. When *CV* is throttling, the pressure drop on the *MSV* is much smaller. The same happens with the *IV* and *ISV*, where due to the large *RH* volume, acts as a cushion, absorbing steam flow ahead of them for several seconds resulting in a negligible effect on throttle flow [16]. But the valves casings are still suffering the thermal stress for the increasing-decreasing temperature in the boiler. However, the temperature is treated to keep it on the nominal temperature with water injection and in this way keep its lifetime on an acceptable number of cycles [17].

Another concern is the vibration on the valves caused by the fast reduction of speed and power while *FV* is acting. Due to several vibration problems in the past, a number of types of *CV* and *IV* have been extensively tested at ALSTOM's factories. The results show that the type of valves for these operations must have

between its features few vibrations for pressure ratios higher than 0.8 for all strokes. When *FV* acts, the range of pressure ratios are within 0.84 and 0.91 [17].

Among others, other potential problems could be also [16]:

- Increased interceptor valve maintenance due to more frequent operation and more severe duty. The increased duty results from the high energy dissipation in the valve when close-opened with full load reheat pressure ahead of the valve. Prime concern is for the large plug type valves on nuclear units which may reach 34 inch nominal size, weighing approximately 25 tons with an overall height of about 20 feet.
- *ISV* may lift on some fossil units depending primarily on *RH* volume. As previously discussed, power operated relief valves of sufficient capacity can be provided to avoid lifting spring loaded safeties. On nuclear units with moisture separator, *RH* volumes in the normal range it is predicted that *ICV* will blow when *FV* occurs above 75% of full load in many cases, unless additional power operated relief valve capacity is supplied.
- On nuclear units, some uncertainty exists regarding the satisfactory design and operation of the complex moisture separator-*RH* drainage system during transient conditions. Difficulties are still being experienced under steady state conditions and it will take some time yet before firm design recommendations can be developed to assure proper operation during transient conditions including *FV* operations.

### *VI.II Mechanical integrity of the turbine*

As was mentioned early, when *FV* is launched, the pressure in the *ST* reaches also higher values than at 100% of the load. This higher pressure has to be considered when the *HP* and *IP* blading are designed, especially the *HP*'s because can have blade factors close to the maximal admissible values. However, it is expected that

the adjustment of the design are only minor, with maybe no influence on the expansion efficiency.

Besides, if power operated relief valves are utilized on the *RH* outlet and automatically opened, periods longer than 11 seconds could be tolerated. It is recommended that specific units being considered for *FV* be analyzed to determine the potential life reduction of the *RH* based on *RH* surface location, flow-interruption time, relief flow, etc [16].

According on some researchers developed by ALSTOM, the critical part is the rotor with *LCF* at the critical locations as rotor notches ($1^{st}$ blade grooves or piston notches). Based on the heat balances, the temperature and pressure variations, the material of the rotor could be chosen less damage suffer and more number of cycle of lifetime without decreasing the performance of the *ST* [17].

# REFERENCES


**[1]** P.Kundur: "*Power System Stability and Control"*, EPRI Powers System Engineering Series, McGraw-Hill, New York, 1994.

**[2]** IEEE Committee Report, "*Dynamic models for steam and hydro turbines in power systems studies*", IEEE Transactions on Power Apparatus and Systems, Vol.PAS-92, No.6, 1973, pp.1904-1915..

**[3]** IEEE Committee Report, *"A study of early valve actuation using detailed prime mover and power system simulation"*, IEEE trans. on Power Systems, Vol. PAS-94, No. 4, 1975.

**[4]** ANSI/IEEE Standard 100-1977: "*IEEE Standard Dictionary of Electrical and Electronics Terms*".

**[5]** IEEE Committee Report: "*Recommended Phasor Diagram for Synchronous Machines*", IEEE Trans., Vol PAS-88, pp. 1593-1610, 1969.

**[6]** Vanfretti, Luigi: "*Modelación y simulación de la máquina síncrona y su operación en sistemas de potencia*", Trabajo de grado presentado a la Facultad de Ingeniería Universidad de San Carlos, Guatemala, mayo de 2005.

**[7]** Electric Machinery Committee of IEEE Power Engineering Society: "*IEEE Std 1110™-2002: Guide for synchronous generator modeling practices and applications in power system stability analysis*", The Institute of Electrical and Electronics Engineers, E.E.U.U. 2003.

**[8]** Díaz Vanegas, Oscar: "*Análisis del amortiguamiento de oscilaciones de baja frecuencia para un sistema de potencia multimáquina*", Trabajo de grado de Maestría en Ingeniería Eléctrica presentado a la Facultad de Ingeniería Eléctrica, Electrónica y Computación de la Universidad Nacional de Colombia, sede Manizales, 2006.

**[9]** Park, R.H: "*Two-Reaction theory of synchronous machines – generalized method of analysis, part I, part II*", AIEE Transactions, Vol. 48: 716-727; Vol. 52: 352-355, E.E.U.U. 1933.

**[10]** Park, R.H: "*Definition of an ideal synchronous machine and formula for the armature flux linkages*", General Electric Vol. 31, Rev. June 1928.

**[11]** Calsan M., De Almeida M. C.: *"Dynamic Performance Analysis of Synchronous Generators Excitation Systems in Distributed Generation Power Plants"*, IEEE paper, Submitted at 03/18/2011 and 1st Revision at 05/20/2011.

**[12]** K. Heuck, K. Dettmann, D. Schulz: *"Elektrische Energieversorgung"*, Vieweg+Teubner Verlag | Springer Fachmedien Wiesbaden GmbH 2010, überarbeitete und aktualisierte Auflage 2010.

**[13]** IEEE Standards Board. "*IEEE recommended practice for excitation system models for power system stability studies*". IEEE Standard, n.421.5-2005, Apr. 2006.

**[14]** IEEE Power Generation Committee of the IEEE: *"Techniques for Tuning Excitation System Parameters"*, Power Engineering SocietyIEEE Transactions on Energy Conversion, Vol. 3, No. 4, December 1988, New York.

**[15]** K. Ogata: *"Modern Control Engineering"*, 3rd Edition, Pearson Education, Practice Hill, Mexico D.F., 1998.

**[16]** E. W. Cushing, Jr, G. E. Drechsler, W. P. Kilgoar, H. G. Marshall, H. R. Stewart: "*Fast Valving as an aid to Power System Transient Stability and Prompt Resynchronization and Rapid Reload After Full Load Rejection"*, Power Generation Committee of the IEEE Power Engineering Society for presentation at the 1971 Joint IEEE-ASME Power Generation Conference, St. Louis, Mo., September 19-23, 1971.

**[17]** ALSTOM Power-Turbo Systems: "*Feasibility Study on ST Assisted Grid Frequency Support"* 30th March 2005, ALSTOM Switzerland.